

A simple model for the evolution of disc galaxies: The Milky Way

Thorsten Naab¹* and Jeremiah P. Ostriker¹

¹Institute of Astronomy, Madingley Road, Cambridge, CB3 0HA, UK

Accepted ??. Received ?? in original form ??

ABSTRACT

A simple model for the evolution of disc galaxies is presented. We adopt three numbers from observations of the Milky Way disc, Σ_d the local surface mass density, r_d the stellar scale length (of the assumedly exponential disc) and v_c the amplitude of the (assumedly flat) rotation curve, and physically, the (local) dynamical Kennicutt star formation prescription, standard chemical evolution equations assuming a Salpeter IMF and a model for spectral evolution of stellar populations. We can determine the detailed evolution of the model with only the addition of standard cosmological scalings with time of the dimensional parameters. A surprising wealth of detailed specifications follows from this prescription including the gaseous infall rate as a function of radius and time, the distribution of stellar ages and metallicities with time and radius, surface brightness profiles at different wavelengths, colours etc. Some of the detailed properties are as follows: the global gas infall rate and the global star formation rate are almost constant at $2-3 M_{\odot} \text{yr}^{-1}$ and $2-4 M_{\odot} \text{yr}^{-1}$ during the evolution of the disc. The present day total mass in stars and in gas is $2.7 \times 10^{10} M_{\odot}$ and $9.5 \times 10^9 M_{\odot}$, respectively, and the disc has an absolute K-band magnitude of -23.2 . The present day stellar scale length (normalised to 3kpc) in the K-band and is larger than at shorter wavelengths. At the solar neighbourhood stars start to form $\approx 10 \text{Gyrs}$ ago at an increasing rate peaking 4 billion years ago and then slowly declining in good agreement with observations. The mean age of long lived stars at the solar neighbourhood is about 4Gyrs . The local surface density of the stars and gas are 35 and $15 M_{\odot} \text{pc}^{-2}$, respectively. The metallicity distribution of the stars at the solar radius is narrow with a peak at $[Z/Z_{\odot}] = -0.1$. The present day metallicity gradient is $-0.046 \text{dex} \text{kpc}^{-1}$ and has been significantly steeper in the past. Using a Chabrier IMF increases the luminosity of the model and results in a steeper metallicity gradient. The local metallicity distribution is only weakly affected. Different formulations for threshold densities for star formation have been tested and lead to a truncation of the stellar disc at about 12kpc . Comparisons with the current and local fossil evidence provides support for the model which can then be used to assess other local disc galaxies, the evolution of disc galaxies in deep optical surveys and also for theoretical investigations such as simulations of merging disc galaxies.

Key words: methods: analytical – galaxies:disc – galaxies: formation – galaxies: evolution – galaxies: fundamental parameters

1 INTRODUCTION

At the present time our knowledge of the current properties of nearby galaxies, including, especially our own Milky Way, far exceeds our ability to model the prior evolution of these systems. Working forwards in time starting with a reasonable cosmological model and computing via *ab initio* methods the evolution at high spatial resolution is a goal

being pursued by many research teams (e.g. Abadi et al. 2003a; Robertson et al. 2004, and references therein) and it may ultimately be successful. However, the project is handicapped by two potentially crippling inadequacies: insufficient numerical resolution and inadequate representation of important physical processes. We shall attempt in this paper to follow an alternative approach which is essentially the inverse of the paradigm described above. We will take as given the present gross properties of our Galaxy: the disc surface mass distribution is exponential and the rotation curve is

* E-mail:naab@ast.cam.ac.uk; jpo@ast.cam.ac.uk

flat. Using these and other properties of normal disc galaxies, we will see if we can construct a prior evolution that ends in this state and is consistent with our knowledge of cosmology. Then we can compare the results with our detailed knowledge of the Galaxy, the distribution of stellar ages and metallicities, to see if our hypothetical evolutionary path is consistent with the present observed state.

The dark matter, largely assembled into self gravitating halos, we take as primary cosmological fact. The distribution of halo masses roughly follows the Press-Schechter distribution

$$\frac{dN(m, t)}{d \ln m} = \left(\frac{2}{\pi}\right)^{1/2} \left(\frac{n+3}{6}\right) \left(\frac{m}{m_*(t)}\right)^{(n+3)/6} \times \exp[(-m/2m_*(t))^{(n+3)/3}] \quad (1)$$

where n is the spectral index of the power spectrum (Lacey & Cole 1994).

Thus, to a good approximation, the evolution of the halo distribution can be computed when the evolution of the nonlinear mass scale $m_*(t)$ is known. This in turn is fixed by the evolution of the linear power spectrum of perturbations $P_\kappa(t) \propto \kappa^n$ since

$$\int_0^{\kappa_{\text{NL}}(t)} P_\kappa(t) \pi \kappa^2 d\kappa = 1 \quad (2)$$

defines the nonlinear wave number κ_{NL} and $m_*(t) = \text{const.} <\rho(t)>/\kappa_{\text{NL}(t)}^3$ at any given n .

Following Lacey & Cole (1994) we note that halos much more massive (at some point in time) than $m_*(t)$ are rare and are being assembled by unusual merger events in isolated high density regions and their number density is rapidly increasing with time. But halos having $m \ll m_*(t)$ have been left behind. They live in lower density regions (or else they would have been merged out of existence) and their numbers are slowly declining.

At the present time the nonlinear halo mass scale is of the order of $10^{14} M_\odot$ but individual halos within which ordinary galaxies live are of order $10^{12} M_\odot$. Thus, these have either been merged into bigger systems (i.e. these halos are now hosts of 'cluster galaxies') which tend to be bulge dominated, or else they live in a lower density 'field' environment and have prominent disc components. Hence if we consider the halo of a system such as our own Milky Way the most likely history was for it to have been assembled via mergers until a time t_f when its mass reached $\approx 10^{12} M_\odot$ corresponding to $m_*(t_f)$. Then it was, for whatever reason (most likely the less than typical density of the larger region surrounding it), side tracked from the cosmic merger dance and survived, with a modest level of subsequent accretion, to the present day. Thus, we take it to have been embedded in a halo with virial velocity v_{vir} which increased with the cosmic typical values $v_{\text{vir}}(t) = v_{\text{vir}}^*(t)$ during the merger phase of its evolution until reaching its current value at t_f after which the galaxy entered its quiet evolutionary phase. The virial velocity remained essentially constant at its present value. The halo, however, still has grown in size and therefore in mass. During the quiet evolutionary phase the gas within the halo can cool and add to the central disc component thereby increasing the inner circular velocity $v_c(r, t)$ due to the increasing disc mass. For simplicity we take $v_c(r, t)$ to be

flat, independent of radius, in accordance with observations of typical spirals and the idea that barygenic infall increases the mass density in the inner parts of galaxies to approximately the level of the maximum of the dark matter rotation curve (Flores et al. 1993).

Since disc galaxies now have close to exponential profiles and there exist several reasonable arguments for how this came about (Mestel 1963; Fall & Efstathiou 1980; Gunn 1982; Dalcanton et al. 1997; Slyz et al. 2002), we will assume that the total surface mass distribution was always exponential with a scale length $r_d(t)$ scaling with the circular velocity as given by spherical infall theory $r_d(t) \propto v_{\text{vir}}(t)/H(t)$. This simple prescription suffices to specify the infall of gas to the disc at all times in the past as a function of both time and radius. Then, if we couple this infall rate with a model for star formation abstracted from observations by Kennicutt (1998), that at each radius 10% of the gas is turned to stars per rotation period, and add a standard treatment of chemical evolution, we have a complete prescription for the evolution of the stellar and gaseous components at every radius. It is amazing that this simple model is able to successfully fit a large number of observational data.

Thus, to summarise, our assumptions are that, after an initial formation period, the disc always maintains an exponential profile with fixed central surface density in a halo providing a flat rotation velocity and the star formation follows a Kennicutt-law. The three numbers known from the present, $r_d(t_0)$, $\Sigma_0(t_0)$, $v_c(t_0)$ fix the final state with $v_{\text{vir}}(t)$ and $\Sigma_0(t)$ held constant and $r_d(t)$ scaling with $1/H(t)$ (see Ferguson et al. 2004 for observational evidence). At early epochs ($t < t_f$), when the scaling relation would give an untypically big and massive system (for the epoch), we simply follow scaling laws of the typical halo at these earlier times.

Over the last decade chemical evolution models have been used to explore the formation of the Galaxy and successfully reproduce properties of the solar neighbourhood, abundance gradients, metallicity distributions, photometric properties etc. (e.g. Beckman & Pagel 1989; Pardi & Ferrini 1994; Pagel & Tautvaišiene 1995; Prantzos & Aubert 1995; Chiappini et al. 1997; Molla et al. 1997; Allen et al. 1998; Prantzos & Silk 1998; Portinari & Chiosi 1999; Boissier & Prantzos 1999; Chang et al. 1999; Hou et al. 2000; Romano et al. 2000; Matteucci & Chiappini 2001; Chiappini et al. 2001; Chang et al. 2002; Casuso & Beckman 2004). Many of these models define the infall rate as a function of time and radius, e.g. exponential in time with e-folding time scales increasing with radius (see e.g. Boissier & Prantzos 1999) or Gaussian-shaped infall rates (Prantzos & Silk 1998) to fit the local properties like gas surface density, abundance gradients or the metallicity distribution. Some authors have used cosmological scaling relations to assess the possible range of present day disc properties. However, the cosmological evolution of the discs with time, which is governed by the infall rate (mostly exponential), has been fixed to fit the present day properties. The infall rates were not directly connected to the cosmological evolution (see e.g. Jimenez et al. 1998; Boissier & Prantzos 2000).

In this paper we follow a different path. We assume that the evolution of the infall rate onto the galaxy is fully constrained by the cosmological model and the small set

of boundary conditions described above and investigate the properties of the resulting galaxy. Those properties are then compared to the Milky Way. We are aware that such a model that is aimed to reproduce global properties of early type discs will probably not be able to reproduce all detailed observations our Galaxy like e.g. colour that depends on the very recent star formation history. On the other side as we consider the Milky Way being a typical spiral galaxy the model has to be able to reproduce its global properties. Given the small number of initial parameters and physical processes involved it is surprising how well the model can reproduce Milky Way properties.

The paper is structured as follows: A review of measurement of the properties of the Milky Way that are used to scale our model are given in Section 2. In Section 3 we describe the details of the model. We develop the scaling relations that determine the infall rate, describe the star formation rule used and the way we have implemented chemical evolution. Our model predictions on the assembly history, the metallicity, and photometric properties are compared to the Milky Way properties in Section 4. The effect of changing the IMF from Salpeter to Chabrier is investigated in Section 5. In Section 6 we investigate the influence of a threshold value for star formation on the outer profiles of the disc and in Section 7 we discuss our results and conclude.

2 PROPERTIES OF THE MILKY WAY

The model for disc galaxy evolution which will be described in Section 3 needs three input parameters: the present day scale length of the total disc surface density distribution $r_d(t_0)$, the central surface density of the disc $\Sigma_d(t_0)$, and the circular velocity $v_c(t_0)$ (assumed to be flat). In this paper we restrict ourselves to a comparison with the Milky Way. This approach has both advantages and disadvantages. If we consider the Milky Way as a typical early type spiral galaxy, any successful model should be able to reproduce the gross properties of its disc. In particular the model has to be able to reproduce data from the solar neighbourhood that mainly depend on the integrated past star formation like the gas and stellar surface mass density and the metallicities of the gas and the stars. Other properties like the colour will directly depend on the very recent star formation history and might not be typical for the mean properties of early type spiral galaxies. Measurements of global properties of the Milky Way like total disc mass and total luminosity suffer from large observational errors. Here the model can help to constrain the data given that it is in agreement with the solar neighbourhood observations.

In this Section we will review the latest observational constraints on the three parameters that we will later use as the input for our model: the scale length of the stellar disc $r_{d,*}$, the circular velocity at the solar neighbourhood v_c and the total surface density of the disc $\Sigma_d(t_0)$ at the solar radius r_\odot .

2.1 Distribution of stars and gas

The stellar disc of the Milky Way is assumed to follow an exponential surface density profile over a wide range in radius. Measurements of the scale length are in the range

$r_{d,*} \approx 2.5 - 3.5 \text{kpc}$ (see Sackett (1997) for a review). More recent investigations report values above as well as below 3kpc , e.g. star counts from the 2MASS survey yield $\approx 3.3 \text{kpc}$ (López-Corredoira et al. 2002) whereas Zheng et al. (2001) get $\approx 2.75 \text{kpc}$ based on direct HST observations of M stars. For the model presented in this paper we therefore assume a conservative value of $r_{d,*} = 3 \text{kpc}$. Several authors find the exponential profile does not fit the outer parts of the Galaxy. They find an edge (truncated stellar emissivity) at $4 - 6 \text{kpc}$ from the Sun (Robin et al. 1992; Ruphy et al. 1996; Freudenhreich 1998). However, López-Corredoira et al. (2002) find no sign for a cut-off in the stellar disc at radii $r < 15 \text{kpc}$. Observations from other disc galaxies clearly indicate an abrupt change in the slope of the stellar profile in more than 60% of the observed disc galaxies at radii of about 3 – 4 times the disc scale length (van der Kruit 1979; van der Kruit & Searle 1981a,b; Pohlen et al. 2000; de Grijs et al. 2001). It has also been proposed that the galactic disc might have an inner hole (Robin et al. 2003).

For the distance of the Sun from the galactic centre we adopt $r_\odot = 8 \text{kpc}$ (Reid 1993) and for the local circular speed we use $v_\odot = 210 \text{km s}^{-1}$ (see Sackett (1997) for a review). Both values are slightly lower but still in agreement with the IAU standards for the galactocentric distance of the Sun and the local circular velocity of $r_\odot = 8.5 \pm 1.1 \text{kpc}$ and $v_\odot = 220 \pm 20 \text{km s}^{-1}$ (Kerr & Lynden-Bell 1986).

The radial distribution of atomic and molecular gas in the Milky Way is shown in Fig. 5. The data from Dame (1993) have been kindly provided by Thomas Dame. The H_2 is more confined to the centre than the HI which can extend to large radii at almost constant surface densities. This is a global feature that is observed for external disc galaxies as well (Young & Scoville 1991). The central depression in HI seems to be common for early-type type disc galaxies like the Milky Way or Andromeda, whereas only about half of them shows a central depression in H_2 (Young & Scoville 1991). We also note that the Galactic H_2 -distribution shows a prominent peak at the centre (Sanders et al. 1984).

2.2 Local surface density

The most reliable measurements have been made for the total mass density within about 1kpc of the Galactic plane. Kuijken & Gilmore (1989, 1991) used spatial and kinematical data of local dwarf stars to determine the vertical gravitational potential and the total mass density (disc + halo) to be $71 \pm 6 M_\odot \text{pc}^{-2}$ within 1.1kpc from the Galactic plane near the Sun. Recently Holmberg & Flynn (2004) reported a similar value for the total dynamical mass within 1.1kpc of $74 \pm 6 M_\odot \text{pc}^{-2}$, $65 \pm 6 M_\odot \text{pc}^{-2}$ within 0.8kpc , and $41 M_\odot \text{pc}^{-2}$ within 0.35kpc . Siebert et al. (2003) determined the total mass density within 0.8kpc to be $76^{+25}_{-12} M_\odot \text{pc}^{-2}$ and Korchagin et al. (2003) determined the dynamical mass within 0.35kpc to be $42 \pm 6 M_\odot \text{pc}^{-2}$.

The determination of which fraction of the matter resides in a flattened disc component or in a flattened or spheroidal halo depends on further assumptions, e.g. the disc scale length, the scale height, the galactocentric distance of the Sun and the distribution of dark matter. Kuijken & Gilmore (1991) found a local disc surface mass density of $48 \pm 9 M_\odot \text{pc}^{-2}$ from modelling the Galactic rotation curve. Some values determined by other stud-

ies depending on additional modelling are $84^{+29}_{-24} M_{\odot} pc^{-2}$ (Bahcall et al. 1992), $52 \pm 13 M_{\odot} pc^{-2}$ (Flynn & Fuchs 1994), or $67^{+47}_{-13} M_{\odot} pc^{-2}$ (Siebert et al. 2003). Recently, Holmberg & Flynn (2004) found $56 \pm 6 M_{\odot} pc^{-2}$ for their disc model.

In contrast to dynamical measurements of the disc surface density, direct observations of the stars at the solar neighbourhood should be less dependent on additional assumptions. Gould et al. (1996) and Zheng et al. (2001) used HST observations of M stars in the Galactic disc to directly determine a surface density of $12.2 - 14.3 M_{\odot} pc^{-2}$. Visible stars other than M stars contribute $\approx 15 M_{\odot} pc^{-2}$, resulting in a total stellar surface density in the range of $\approx 27 - 30 M_{\odot} pc^{-2}$. Alternatively, star counts within $5 pc$ of the Sun using *Hipparcos* parallaxes (Jahreiß & Wielen 1997) combined with the observed vertical disc profile (Zheng et al. 2001) give a similar number of $26.9 M_{\odot} pc^{-2}$ (Binney & Evans 2001). With a local gas surface density (the one we assume here is slightly higher than the one derived by Dame 1993) of $\approx 13 - 14 M_{\odot} pc^{-2}$ (Bahcall et al. 1992; Olling & Merrifield 2001) the total mass density of the disc would lie in the range of $40 - 44 M_{\odot} pc^{-2}$. Interestingly, those measurements give surface densities that lie significantly below the dynamical estimates. As the effect of binary stars is supposed to be small (Gould et al. 1996) the difference might be caused by undetected dead stellar remnants and brown dwarfs. These we estimate to $5 - 7 M_{\odot} pc^{-2}$, to give a total surface density of $45 - 51 M_{\odot} pc^{-2}$.

Independent of which number is closer to the truth there is a discrepancy between the amount of identified disc matter and the total column density within $1.1 kpc$ of about $20 - 35 M_{\odot} pc^{-2}$ which could be attributed to a spheroidal dark matter component. The exact amount of dark matter in the solar neighbourhood is unknown. Most authors find no evidence for dark matter in the disc at the solar radius (Kuijken & Gilmore 1991; Holmberg & Flynn 2004). (However, taking the dynamical measurements and the direct observations at face value $10 - 15 M_{\odot} pc^{-2}$ could reside in a dark disc component, see next Section)

Throughout the paper our model is constrained to have a total mass surface density of the baryonic disc components (stars + gas) within $|z| < 1.1 kpc$ at the solar radius $r_{\odot} = 8 kpc$ of $50 M_{\odot} pc^{-2}$. The division between live stars, stellar remnants and gas is determined by the computation.

3 THE MODEL FOR DISC GALAXY EVOLUTION

In this Section we describe the theoretical framework we need to model the formation and evolution of an early type galactic disc.

3.1 Disc scalings

We assume that in the absence of star formation the gas in a given halo would settle in a disc with an exponential surface density

$$\Sigma_d(r, t) = \Sigma_0(t) \exp(-r/r_d(t)), \quad (3)$$

where the central surface density Σ_0 and the scale length r_d change with time. The cumulative mass distribution of the disc is

$$M_d(r, t) = M_d(t)(1 - (1 + r/r_d) \exp(-r/r_d)), \quad (4)$$

where

$$M_d(t) = 2\pi\Sigma_0(t)r_d^2(t) \quad (5)$$

is the total mass of the disc. In the limit of a thin disc its rotational velocity is given by

$$v_d^2(r, t) = 4\pi G\Sigma_0(t)r_d(t)y(r, t)^2[I_0(y)K_0(y) - I_1(y)K_1(y)], \quad (6)$$

where G is the gravitational constant, $y(r, t) = r/(2r_d(t))$ and $I_i(y)$ and $K_i(y)$ are the modified Bessel functions of the first and second kind (Freeman 1970). Real discs have a finite thickness and a slightly lower rotation velocity. The effect is, however, small and will not affect the results presented here. The rotation velocity of the disc peaks at $r_{2.2}(t) = 2.15r_d(t)$ at a value of

$$v_{d,2.2}^2(t) = 0.774\pi G\Sigma_0(t)r_d(t) \quad (7)$$

with $y = 1.075$ in Eqn. 6. The disc material within $r_{2.2}$ accounts to 64.5% of the total mass of the disc (Eqn. 4). At $r_{2.2}(t)$ the disc contributes a fraction of

$$f_v(t) = v_{d,2.2}(t)/v_c(t) \quad (8)$$

to the circular velocity $v_c(t)$ which is assumed to be constant with radius. In general, f_v can vary with time. The exact value of f_v for present day disc galaxies is still under debate. If galactic discs were maximum then $f_v = 0.85 \pm 0.1$ at $r_{2.2}$ which seems to be close to correct for the Milky Way (Sackett 1997). However, using data from nearby disc galaxies Courteau & Rix (1999) favour a value of $f_v = 0.6 \pm 0.1$ which is in good agreement with the value of $f_v = 0.63$ derived by Bottema (1993). Our adopted model has a present day value of $f_v = 0.61$ (see Fig. 1).

Using the above scalings we can estimate the total mass in dark matter (assuming a spherical distribution, e.g. the dark matter does not concentrate significantly in the disc) inside $r_{2.2}$ using

$$v_c^2 = v_{dm}^2 + v_d^2 = \frac{GM_{dm}(r_{2.2})}{r_{2.2}} + v_d^2. \quad (9)$$

as

$$M_{dm}(r_{2.2}) = \frac{r_{2.2}}{G} v_c^2 (1 - f_v^2) \quad (10)$$

which gives $4.3 \times 10^{10} M_{\odot}$ ($1.9 \times 10^{10} M_{\odot}$) for $f_v = 0.6$ ($f_v = 0.85$). Assuming a constant density of a spherical dark matter halo up to the solar radius (Binney & Evans (2001) argue that no halo with a cusp steeper than $r^{-0.3}$ is viable) we can estimate the column density within $z_{1.1} = 1.1 kpc$ using

$$\Sigma_{dm}(r_{2.2}) = \frac{1}{4\pi Gr_{2.2}^2} v_c^2 (1 - f_v^2) z_{1.1}. \quad (11)$$

With $r_{2.2} = 6.6 kpc$, $v_c = 210 km s^{-1}$ and $f_v = 0.6$ this would result in a dark matter surface density of $26.4 M_{\odot} pc^{-2}$ or $11.3 M_{\odot} pc^{-2}$ for the maximum disc case ($f_v = 0.85$) and leave $45 - 60 M_{\odot} pc^{-2}$ for the disc itself, assuming the Kuijken & Gilmore (1991) value of $71 M_{\odot} pc^{-2}$.

Table 1. Predicted local properties of model and observations of the Milky Way at the solar neighbourhood

| Observable | Model | Observed values | Reference |
|---|-------|------------------|----------------------------|
| Total surface density from stellar dynamics | | | |
| $ z < 1.1kpc, [M_{\odot}pc^{-2}]$ | | 71 ± 6 | Kuijken & Gilmore (1991) |
| | | 74 ± 6 | Holmberg & Flynn (2004) |
| $ z < 0.8kpc$ | | 76^{+25}_{-12} | Siebert et al. (2003) |
| $ z < 0.35kpc$ | | 65 ± 6 | Holmberg & Flynn (2004) |
| | | 42 ± 6 | Korchagin et al. (2003) |
| | | 41 | Holmberg & Flynn (2004) |
| Total disc surface density from disc modelling | | | |
| $[M_{\odot}pc^{-2}]$ | 50 | 46 ± 9 | Kuijken & Gilmore (1989) |
| | | 48 ± 9 | Kuijken & Gilmore (1991) |
| | | 84^{+29}_{-24} | Bahcall et al. (1992) |
| | | 52 ± 13 | Flynn & Fuchs (1994) |
| | | 56 ± 6 | Holmberg & Flynn (2004) |
| Surface density of visible stars from direct observations | | | |
| $[M_{\odot}pc^{-2}]$ | 32 | 35 ± 5 | Gilmore et al. (1989) |
| | | 27 | Gould et al. (1996) |
| | | 30 | Zheng et al. (2001) |
| Surface densities of stellar remnants | | | |
| $[M_{\odot}pc^{-2}]$ | 3 | 2 – 4 | Mera et al. (1998) |
| Gas surface densities from direct observations | | | |
| $[M_{\odot}pc^{-2}]$ | 15 | 8 ± 5 | Dame (1993) |
| | | $13 - 14$ | Olling & Merrifield (2001) |
| Star formation rate | | | |
| $[M_{\odot}pc^{-2}Gyr^{-1}]$ | 6.4 | 2-10 | Guesten & Mezger (1982) |
| | | 3.5-5 | Rana (1991) |
| Infall rate | | | |
| $[M_{\odot}pc^{-2}Gyr^{-1}]$ | 3.3 | | |
| Luminosities | | | |
| $L_B[L_B\odot pc^{-2}]$ | 38 | 20 ± 2 | van der Kruit (1986) |
| $L_V[L_V\odot pc^{-2}]$ | 30 | 22.5 ± 3 | Pagel (1997) |
| $L_K[L_K\odot pc^{-2}]$ | 59 | 68 ± 23 | Kent et al. (1991) |

Table 2. Some observed global properties of the Milky Way and model predictions

| Observable | Model | Observed values | Reference |
|--|-------|--|--|
| Star formation rate $[M_{\odot}yr^{-1}]$ | 3.6 | 0.8 - 13 3.5-5 | Rana (1991) for references Rana (1991) |
| Infall rate $[M_{\odot}yr^{-1}]$ | 2.2 | 0.5 - 5 | Braun & Thilker (2004) |
| Total luminosities | | | |
| $L_B[L_B\odot]$ | 2.4 | $1.8 \pm 3 \times 10^{10}$ | van der Kruit (1986) |
| $L_V[L_V\odot]$ | 1.9 | $(1.4 < L_V\odot < 2.1) \times 10^{10}$ 1.24×10^{10} 2.1×10^{10} | van der Kruit (1986) Bahcall & Soneira (1980) Sackett (1997) |
| $L_K[L_K\odot]$ | 4.1 | 4.9×10^{10} | Kent et al. (1991) |

3.2 Cosmological scalings

During the self-similar structure formation process, the time evolution of the halo depends on the assumed cosmology. In the spherical collapse model (Gunn & Gott 1972; Bertschinger 1985; Cole & Lacey 1996) the virial radius r_{vir} and the virial mass M_{vir} (the mean density within r_{vir} is $200\rho_{\text{crit}}$) of a halo with virial velocity v_{vir} at any time t is given approximately by

$$r_{\text{vir}}(t) = \frac{v_{\text{vir}}(t)}{10H(t)}, \quad M_{\text{vir}} = \frac{v_{\text{vir}}^3(t)}{10GH(t)} \quad (12)$$

with

$$H[z(t)] = H_0[\Omega_{\Lambda,0} + (1 - \Omega_{\Lambda,0} - \Omega_0)(1+z)^2 + \Omega_0(1+z)^3]^{1/2}, \quad (13)$$

where $H(z)$ is the Hubble parameter at redshift z (see also Mao et al. (1998)). We chose $h = 0.70$ and $\Omega_0 = 0.30$ for a closed universe as constrained recently by *WMAP* and *SDSS* data (Tegmark & et al. 2004).

We assume that the formation and evolution of a typical disc galaxy proceeds in two phases. At early cosmic times the galaxy follows the general cosmological evolution, e.g. we have estimated the evolution of the circular velocity by calculating the redshift at which the value of the Press-Schechter mass function is maximum for a given halo mass (Antonio Vale, private communication). In other words, we take the peak circular velocity of the most common halo at every epoch. At the time a halo reaches its present day virial velocity the second phase starts which is the dominant phase of disc growth. We assume that the halo decouples from the general cosmological evolution and its virial velocity will stay constant from then on:

$$v_{\text{vir}}(t < t_{\text{form}}) = v_{\text{vir}}(t) \text{ of most common halo} \quad (14)$$

$$v_{\text{vir}}(t \geq t_{\text{form}}) = v_{\text{vir}}(t_{\text{form}}). \quad (15)$$

We call this time the formation time t_{form} of the halo. For simplicity we assume that the virial velocity of the galaxy is flat at all radii.

We now assume that the scale length r_d of the gas disc forming within a given halo is a fixed fraction f_r of the virial radius r_{vir} of the halo,

$$r_d(t < t_{\text{form}}) = f_r r_{\text{vir}}(t) = f_r \frac{v_{\text{vir}}(t)}{10H(t)} \quad (16)$$

$$r_d(t \geq t_{\text{form}}) = f_r \frac{v_{\text{vir}}(t_{\text{form}})}{10H(t)} = r_d(t_{\text{form}}) \frac{H(t_{\text{form}})}{H(t)}. \quad (17)$$

After its formation time the virial radius of the halo and its total mass do still increase according to Eqn. 12. The circular velocity, v_c , at the inner parts of the halo is now corrected for the disc component that is building up,

$$v_c^2(t \geq t_{\text{form}}) = v_{\text{vir}}^2(t_{\text{form}}) + v_{d,2.2}^2(t). \quad (18)$$

For simplicity we do not take the effect of the adiabatic contraction of the dark matter halo into account.

In the upper panel of Fig. 1 we show the evolution of the circular velocity of the disc galaxy. Initially it follows the evolution of the most common halo at every epoch. At the formation time, $t_{\text{form}} \approx 2.5 \text{Gyrs}$, the halo decouples from the cosmological evolution and the circular velocity increases due to growth of the disc to its present day value of 210km s^{-1} . As shown in the second panel of Fig. 1 the disc scale length evolves according to Eqn. 16 and 17, assuming

$f_r = 1/70$. This value has been chosen to guarantee the the final stellar scale length is 3kpc . The scaling implies that the total disc angular momentum $J(t) \propto M v_c r_d$ scales with the expected angular momentum of the infalling gas.

Combining Eqns. 7, 8 and 16 we obtain an expression for the evolution of the central surface density of the disc. At times earlier than t_{form} we keep $f_v = \text{const.}$ and let the central surface density increase; after t_{form} we keep the central surface density fixed as the infalling gas will have a too large angular momentum to fall to the centre. As a result, f_v will begin to increase as $f_v \propto H^{-1/2}$:

$$\Sigma_0(t < t_{\text{form}}) = \frac{1}{0.774\pi G} \frac{f_v^2(t)}{f_r} 10H(t)v_{\text{vir}}(t), \quad (19)$$

$$f_v(t < t_{\text{form}}) = \text{const.}, \quad (20)$$

and

$$\Sigma_0(t \geq t_{\text{form}}) = \Sigma_0(t_{\text{form}}), \quad (21)$$

$$f_v^2(t \geq t_{\text{form}}) = 0.774\pi G \frac{f_r \Sigma_0(t_{\text{form}})}{10H(t)v_c(t)}. \quad (22)$$

In the third panel of Fig. 1 we show the evolution of the central surface density of the disc. The system has been scaled according to a present day total disc surface density of $50 M_{\odot} \text{pc}^{-2}$ at $r = 8 \text{kpc}$, resulting in $f_v = 0.36$ at t_{form} (see Section 2 for the parameters assumed for the Milky Way). For times $t < t_{\text{form}}$, f_v has been kept fixed at this value, at $t \geq t_{\text{form}}$, f_v is increasing according to Eqn. 22 to a present day value of $f_v = 0.61$ (see last panel in Fig. 1).

By now the total surface density profile of the disc is known at any time (Eqn. 3). Therefore the surface density of the infall rate is given by

$$\Sigma_{\text{IFR}}(r, t) = \frac{\Sigma_d(r, t + dt) - \Sigma_d(r, t)}{dt}. \quad (23)$$

To summarise, the evolution of the infall rate of the disc is fully constrained by three present day parameters: the circular velocity of the disc, the disc scale length (defined by f_r), and the central surface density of the disc (defining f_v at t_{form}).

3.3 Star formation law

At this point we have to include a model for star formation to the model to follow the evolution of the stellar and gaseous phase separately. After the gas within a halo has settled into a disc it starts forming stars. Kennicutt (1998) has given two alternative formulations that successfully describe the relation between the averaged surface density of the star formation rate (SFR) and the averaged total gas surface density in observed disc galaxies. The first can empirically be parametrised by a simple Schmidt-type law

$$\Sigma_{\text{SFR}} \propto \Sigma_{\text{gas}}^n, \quad (24)$$

where on average $n \approx 1.4$. The SFR surface density of individual galaxies can, however, deviate by a factor of 7 from this relation. The second formulation, which seems, empirically, equally valid, and is more physically motivated, is

$$\Sigma_{\text{SFR}} \propto \frac{\Sigma_{\text{gas}}}{\tau_{\text{dyn}}}, \quad (25)$$

where τ_{dyn} is the dynamical time of the system ($\propto \Omega^{-1}$). A law of this kind was predicted in case the passage of spi-

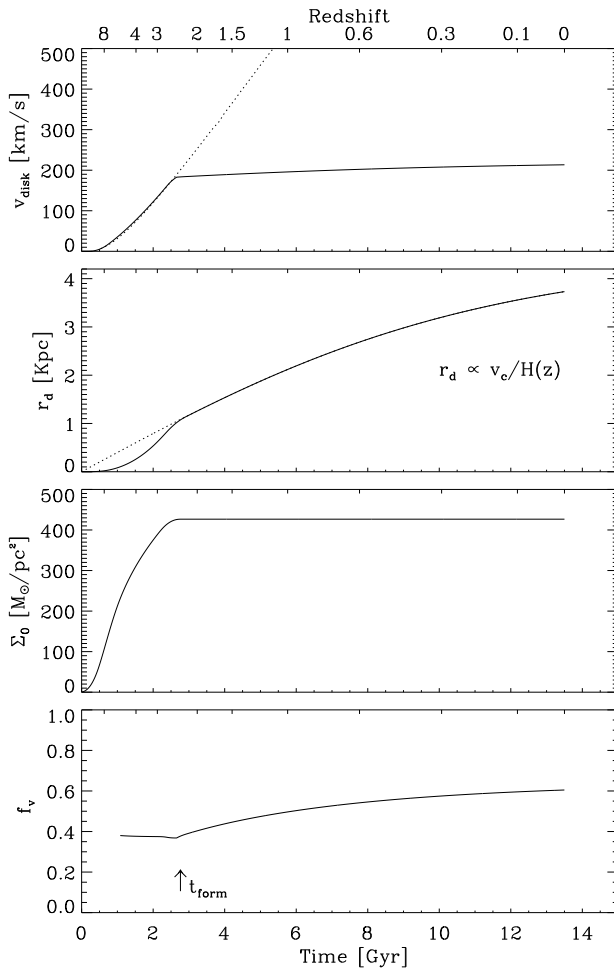


Figure 1. *Upper panel:* Circular velocity v_c of the model galaxy versus cosmic time (solid line). The dashed line shows the peak circular velocity of the most common halo at every epoch. The galaxy halo reaches its final circular velocity ($\approx 190 \text{ km s}^{-1}$) at the formation time $t_{\text{form}} \approx 2.5 \text{ Gyr}$ (indicated by an arrow in the lowest panel). Thereafter v_c increases due to the growth of the disc to its final value of $v_c = 210 \text{ km s}^{-1}$. *Second panel:* Evolution of the scale length with cosmic time according to Eqns. 16 and 17, assuming $f_r = 1/70$ (solid line). The dashed line for comparison shows the evolution for $r \propto H^{-1}$. *Third panel:* Total central surface density of the disc versus time according to Eqn. 19 and 21 scaled to the Milky Way value at $t = t_{\text{form}}$ and kept constant thereafter. *Lowest panel:* Time evolution of f_v (Eqns. 20 and 22).

ral arms plays an important role triggering star formation (Wyse & Silk 1989). In the original formulation, Kennicutt (1998) found that on average 21% of the available total gas mass per orbit within the outer edge of the disc is transformed into stars, or

$$\Sigma_{\text{SFR}} = \epsilon \frac{\Sigma_{\text{gas}}}{\tau_{\text{orb}}}, \quad (26)$$

where $\tau_{\text{orb}} = 2\pi r_{\text{out}}/v_c$ is the orbital period at the outer radius r_{out} and $\epsilon \approx 0.1$ (Kennicutt 1998) is the star formation efficiency. Alternatively this relation can be written as

$$\tau_{\text{orb}} = \epsilon \tau_{\text{gas}}, \quad (27)$$

where $\tau_{\text{gas}} = \Sigma_{\text{gas}}/\Sigma_{\text{SFR}}$ is the time scale for the depletion of gas by star formation.

Throughout this paper we use a formulation based on the local dynamical time (rotation period) of the system. At every radius the surface density of the star formation rate is given by

$$\Sigma_{\text{SFR}}(r, t) = \epsilon \frac{\Sigma_{\text{gas}}(r, t)}{\tau_{\text{orb}}(r, t)} \quad (28)$$

with

$$\tau_{\text{orb}}(r, t) = \frac{2\pi r}{v_c(t)} \quad (29)$$

and a star formation efficiency of $\epsilon = 0.1$. Wong & Blitz (2002) have tested the validity of the above local formulations, which were originally derived from disc averaged data, for individual discs using azimuthally averaged data of a sample of molecule-rich spirals. They find that the parametrisations based on a local Schmidt-law and on the local dynamical time of the systems are both consistent with observations. Boissier et al. (2003) who in addition tested one further parameterisation proposed by (Dopita & Ryder 1994)

$$\Sigma_{\text{SFR}} = \alpha \Sigma_{\text{gas}}^n \Sigma_{\text{T}}^m, \quad (30)$$

where Σ_{T} is the total surface density, that is sometimes used in chemical evolution models (Matteucci & Chiappini 2001) find a good agreement with the Milky Way data for all three formulations (however with different values for the exponents m and n than Dopita & Ryder (1994)). In particular, they find a good agreement assuming a flat rotation curve for the Milky Way.

It is not surprising that the above simple prescriptions for star formation that depend on the gas density itself fit the observed data reasonably well. All algorithms which maintain a relatively moderate ratio of gas to stars will lead to the same results.

3.4 Chemical evolution

We follow the evolution of the model galaxies in independent rings assuming no radial gas flows using a modified version of the chemical evolution model of Ostriker & Tinsley (1975). In every independent ring the change in gas surface density Σ_{g} and surface density in stars Σ_{s} is given by

$$\begin{aligned} d\Sigma_{\text{g}}(r, t) &= -\Sigma_{\text{SFR}}(r, t)dt + K_{\text{ins}}(r, t)dt \\ &\quad + K_{\text{late}}(r, t)dt + \Sigma_{\text{IFR}}(r, t)dt \end{aligned} \quad (31)$$

$$\begin{aligned} d\Sigma_{\text{s}}(r, t) &= \Sigma_{\text{SFR}}(r, t)dt - K_{\text{ins}}(r, t)dt \\ &\quad - K_{\text{late}}(r, t)dt, \end{aligned} \quad (32)$$

where Σ_{SFR} is the star formation rate per unit area (Eqn. 28) and Σ_{IFR} is the rate of gas infall onto the galaxy per unit area, as defined in Eqn. 28. K_{ins} is the mass per unit area in gas ejected from massive stars instantaneously, K_{late} is the mass per unit area in gas ejected at later evolutionary phases of low mass stars. They are defined as

$$K_{\text{ins}}(r, t) = R_{\text{ins}} \Sigma_{\text{SFR}}(r, t), \quad (33)$$

$$K_{\text{late}}(r, t) = \int_0^t \Sigma_{\text{SFR}}(t', r) W(t - t') dt'. \quad (34)$$

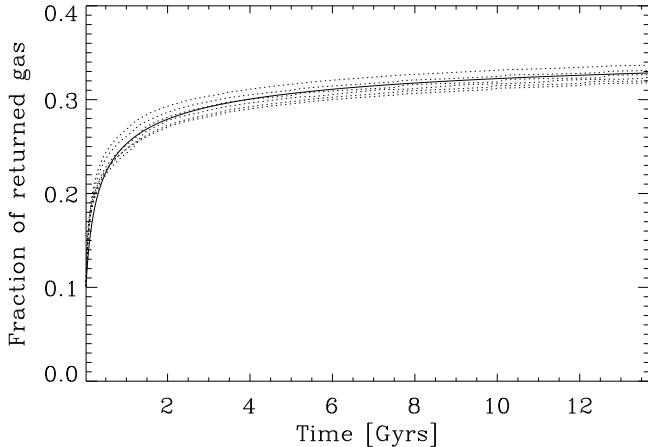


Figure 2. Fraction of mass lost from a single burst population of stars versus time according to Eqns. 33 and 34 for a Salpeter IMF (solid line) which is a good approximation to the metal dependent value of Bruzual & Charlot (2003) shown by the dashed lines for $0.0001 < Z < 0.05$.

Table 3. Input parameters for the Milky Way disc model

| Input parameters | |
|---|---|
| Solar radius | $r_\odot = 8\text{kpc}$ |
| Circular velocity at r_\odot | $v_c = 210\text{km}\text{s}^{-1}$ |
| Total disc surface density at r_\odot | $\Sigma_\odot = 50M_\odot\text{pc}^{-2}$ |
| Disc collapse fraction | $f_r = 1/70$ |
| Star formation IMF | Salpeter |
| Star formation efficiency | $\epsilon = 0.1$ |
| Solar metallicity | $Z_\odot = 0.0126$ |
| Effective yield | $Y = 0.0095 - 0.0135$ |
| Z of infalling gas | $Z_{\text{IF}} = 1 \times 10^{-4} - 3.7 \times 10^{-3}$ |

$R_{\text{ins}} = 0.1$ is the fraction of gas returned instantaneously to the ISM from newborn massive stars and $W(t)$ is a weighting function defined as

$$W(t) = R_* \frac{\delta_* - 1}{\tau_0} \left(\frac{\tau_0}{t + \tau_0} \right)^{\delta_*} \quad (35)$$

with $R_* = 0.3$, $\delta_* = 1.36$, and $\tau_0 = 1 \times 10^8$ assuming a Salpeter (1955) IMF (Ciotti et al. 1991). This analytic expression is a good approximation (see Fig. 2) for the fraction of returned gas for a single burst population to the metal dependent values of the spectral evolution model by Bruzual & Charlot (2003) that we have used to compute the photometric properties of the model disc (see Section 4.4). The evolution of the mass of metals in the gas z_g follows

$$\begin{aligned} \Sigma_g(r, t) dz_g &= Y(1 - z_g(r, t)) \Sigma_{\text{SFR}}(r, t) dt \\ &+ (z_{\text{IF}} - z_g(r, t)) \Sigma_{\text{IFR}}(r, t) dt \\ &+ \int_0^{t'} [z_g(r, t') - z_g(r, t)] \Sigma_{\text{SFR}}(r, t') W(t - t') dt' dt \end{aligned} \quad (36)$$

where Y , the yield, is the mass fraction of newly formed metals of the total mass of gas returned to the ISM. z_{IF} is the metallicity of the infalling gas (see Section 4.3).

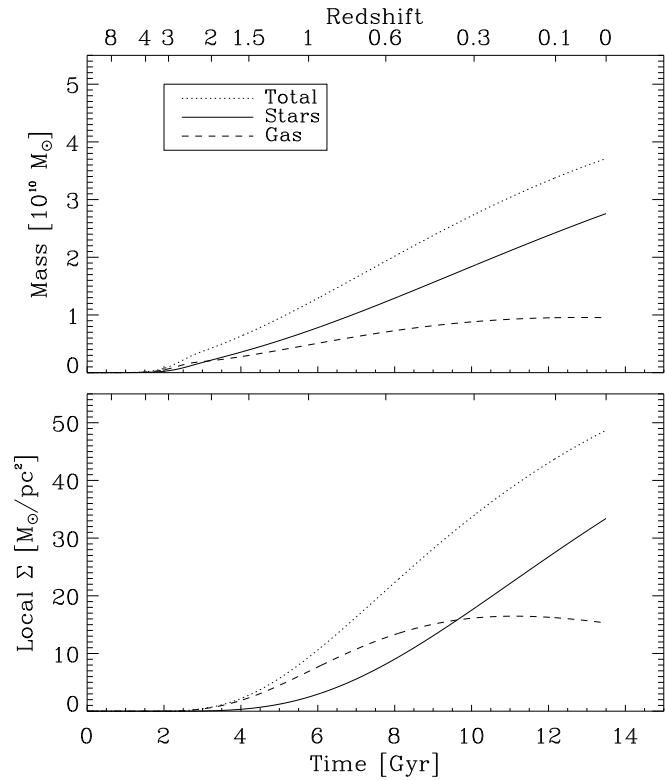


Figure 3. *Upper panel:* Time evolution of the total mass, the mass in stars and the mass in gas for the model disc. *Lower panel:* Time evolution of the total surface density, the stellar surface density and the gas surface density at the solar radius.

4 MODEL PROPERTIES AND COMPARISON TO THE MILKY WAY

In this section we present the properties of the galactic model disc assuming the present day properties of the Milky Way discussed in Section 2 and the evolutionary model of Section 3. All input parameters are summarised in Table 3. In addition, we compare the model disc to available global and local observed properties of the Milky Way.

4.1 Mass assembly

The upper panel in Fig. 3 shows the evolution of the total disc mass in gas and stars, respectively. The total mass of the disc out to 26kpc is $M_{\text{tot}} = 3.7 \times 10^{10} M_\odot$ with about $M_g = 9.5 \times 10^9 M_\odot$ in gas and $M_{\text{tot}} = 2.7 \times 10^{10} M_\odot$ in stars. These values are in good agreement with mass models for the Milky Way by Dehnen & Binney (1998) that are based on observational constraints. For $r_d = 8\text{kpc}$ and $r_d/r_\odot = 0.375$ they would predict a total disc mass (ISM + thick stellar disc + thin stellar disc) in the range of $3 - 4.5 \times 10^{10} M_\odot$ depending on additional theoretical constraints. Bahcall & Soneira (1980) estimated the stellar mass of the disc to be $2.0 \times 10^{10} M_\odot$.

The time evolution of the local surface density is shown in the lower plot in Fig. 3. The model has been normalised to a present day total surface density of $50 M_\odot \text{pc}^{-2}$. The gas starts to assemble at the solar radius after 3Gyrs , and after

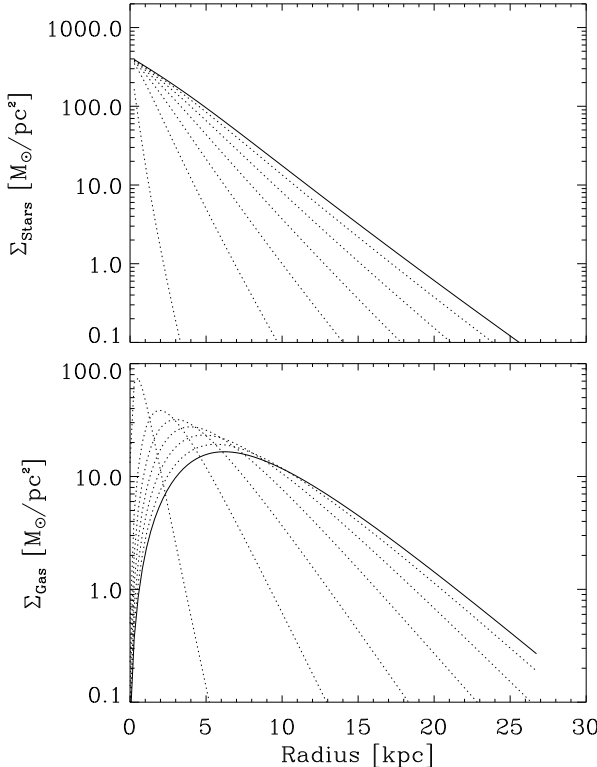


Figure 4. Stellar surface density profiles (upper panel) and gas surface density profiles (lower panel) at 2, 4, 6, 8, 10, 12, and 13.6 Gyrs (as indicated in Fig. 3 for the solar radius). The present day profile is shown by the thick lines.

6Gyrs the local gas surface density stays almost constant at its present day value of $15M_{\odot}/pc^{-2}$ in good agreement with the observed $13 - 14M_{\odot}/pc^{-2}$. The first stars at the solar radius form after 4Gyrs followed by a steady increase to the present day value of $35M_{\odot}/pc^{-2}$ (with $\approx 3M_{\odot}/pc^{-2}$ invisible in stellar remnants) resulting in $\approx 32M_{\odot}/pc^{-2}$ visible stars which is only slightly higher than the value of $27 - 30M_{\odot}/pc^{-2}$ derived from direct observations of normal stars (see Section 2.2 for discussion).

The time evolution of the surface density profile for stars and gas is shown in Fig. 4 and reveals the inside out formation of the stellar disc, originally suggested by Matteucci & Francois (1989). The stellar profile is always close to exponential with increasing scale lengths with time. The gas profile develops a central depression with an exponential outer profile. The present day profiles are indicated by thick lines. In Fig. 5 we show in addition the present day total surface density profile, which is an exponential by definition. The stellar profile is very close to exponential in the outer parts, however, with a smaller scale length. The gas is almost depleted at the centre. The surface density is rapidly increasing with radius and reaches a maximum at 7kpc. Thereafter it decreases almost exponentially with a scale length significantly larger than the one of the stars and of the total surface density. The gas distribution of the model disc compares well with the observed one (lower panel in Fig. 5). The peak, however, is at a slightly larger radius (7kpc compared to the observed 5kpc). We have to note that

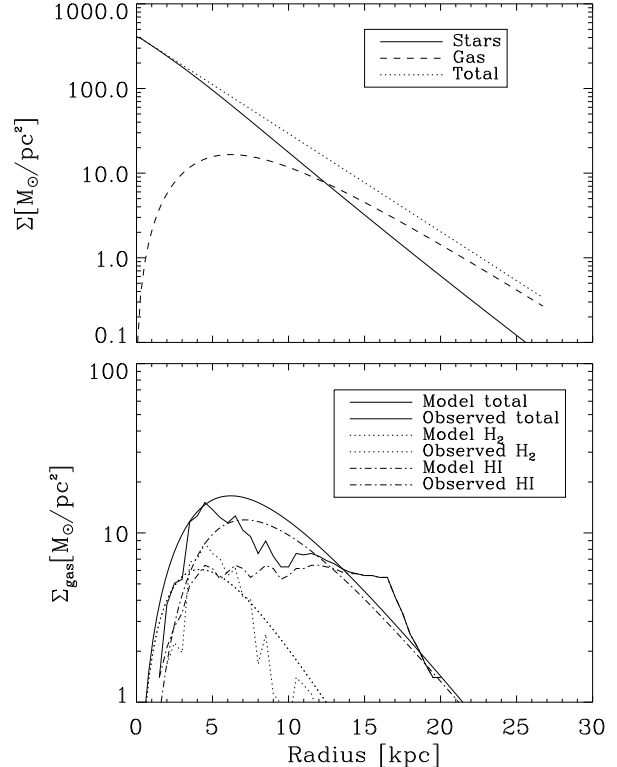


Figure 5. *Upper plot:* Final surface density distributions of the total baryonic matter (dashed), stars (solid) and gas (dotted). *Lower plot:* Observed surface density distribution for H_2 (dotted thin), HI (dot-dashed thin), and $H_2 + HI$ (solid thin) increased by a factor of 1.4 to account for Helium and heavier elements. The data has been kindly provided by Thomas Dame (Dame 1993). The thick solid line is the model prediction for the total gas density. The thick dotted (thick dot-dashed) line indicates the model prediction for H_2 (HI) assuming $\Sigma_{HI}/\Sigma_{H_2} \propto r^{-1}$ (Wong & Blitz 2002).

we did not explicitly include a central bulge (bar) component to the model which might have a strong influence on the evolution of the gas profile in the inner parts, e.g. star formation close to the centre might be suppressed and the Milky Way bar might induce gas inflow towards the centre. Therefore the profile at small radii is not to be over-interpreted. It is, however, surprising that we get a reasonable fit without a detailed modelling of the bulge. Of course, by assuming a flat rotation curve into the centre we are, dynamically, implicitly allowing for a steep bulge component since the rotation due to the disc alone would be linear ($v_d \propto r$).

4.2 Infall and star formation history

The time evolution of the radial distribution of the surface density of the star formation rate and the infall rate (see Eqn. 23) for the modelled galactic disc leading to the inside out formation is shown in Fig. 6. At early times the star formation rate is centrally concentrated and can locally exceed $100M_{\odot}/pc^{-2}Gyr^{-1}$. At later evolutionary phases the gradient flattens and star formation occurs over a large range in radius. In Fig. 7 we compare the time evolution of the infall

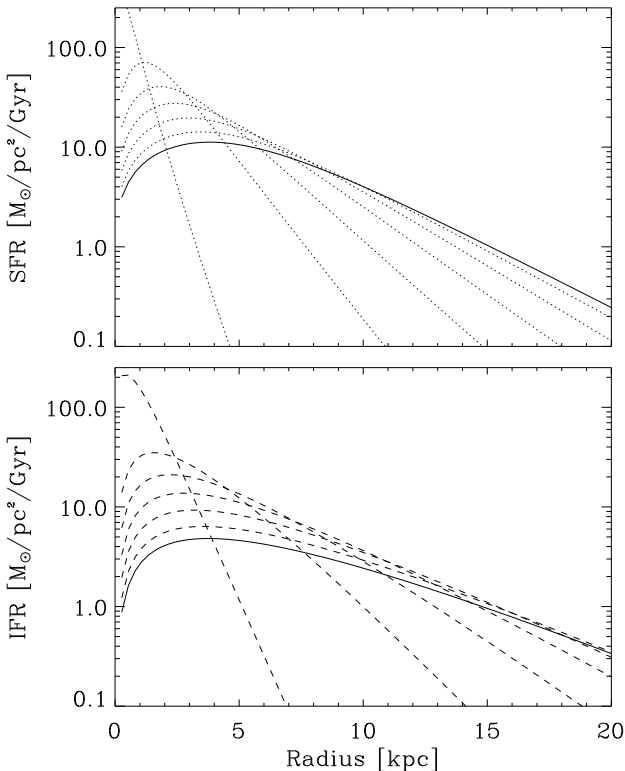


Figure 6. Star formation rate (upper panel) and infall rate (lower) versus radius. Data are shown at 2, 4, 6, 8, 10, 12, and 13.6 (thick line) *Gyrs*.

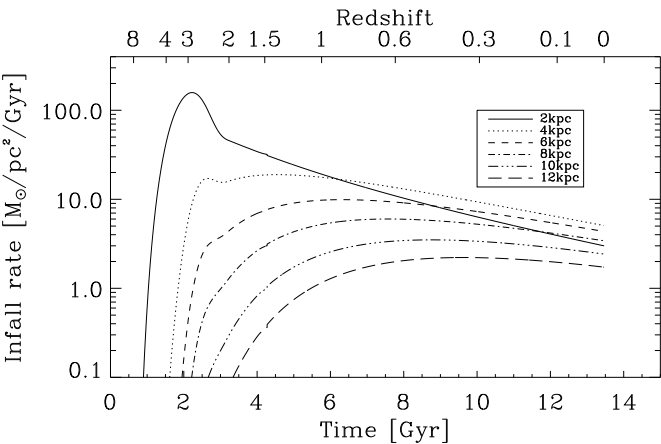


Figure 7. Infall rate of the model versus time at different radii.

rate at different radii. The evolution of the total star formation and infall rate of the model galaxy is shown in the upper plot of Fig. 8. Both distributions are very broad indicating almost constant rates over a long period of time. The star formation rate had its maximum ≈ 3 *Gyrs* ago which is in reasonably good agreement with star formation histories of galaxies of a similar mass (peaks between 2 and 3 *Gyrs*) determined by the analysis of the 'fossil record' of nearby galaxies (Heavens et al. 2004). The present day global value is $3.6 M_{\odot} pc^{-2} Gyr^{-1}$.

The infall rate onto the galaxy over the last 10*Gyrs* in the range of $2 - 4 M_{\odot} yr^{-1}$ varies only weakly and has a present day value of $2.2 M_{\odot} yr^{-1}$. This is in excellent agreement with estimates of infall rates of $1 - 3 M_{\odot} yr^{-1}$ that would be able to compensate for the rapid molecular-gas depletion in the Milky Way disc (Lacey & Fall 1985). Observationally, a strong indication for the importance of infall is the significant presence of Deuterium at the solar neighbourhood (Linsky 2003) as well as at the galactic centre (Lubowich et al. 2000). As Deuterium is destroyed in stars and as there is no other known source of deuterium in the Galaxy it is cosmological and of extragalactic origin (Ostriker & Tinsley 1975; Lubowich et al. 2000). Chemical evolution models that have followed the evolution of Deuterium find values consistent with observations (Tosi et al. 1998; Chiappini et al. 2002). A significant fraction of infalling low metallicity gas could be high velocity clouds (HVCs) that have been accreted onto the Milky Way disc and supply the ISM with Deuterium (Sembach et al. 2004). Inferred HVC infall rates of between $0.5 M_{\odot} yr^{-1}$ and $5 M_{\odot} yr^{-1}$ (Wakker et al. 1999; Blitz et al. 1999; Braun & Thilker 2004) are also in good agreement with indirect evidence from recent chemical evolution models that imply an average (and constant or even slowly rising) accretion rate of $\approx 1 - 2 M_{\odot} yr^{-1}$ (see e.g. Giovagnoli & Tosi (1995); Casuso & Beckman (2004) and references therein). This is particularly interesting as other successful models for the Milky Way use exponentially decreasing infall rates (Chiappini et al. 1997; Boissier & Prantzos 1999).

Another independent estimate of the global infall rate based on the type II supernovae rates of the Milky Way of $\approx 2 - 5 century^{-1}$ (e.g. Cappellaro et al. 1993; van den Bergh & McClure 1994; Tammann et al. 1994; Dragicevich et al. 1999) would result in a similar accretion rate for a Salpeter IMF (Casuso & Beckman 2004). This is in good agreement with the SNII rate derived from the model of $\approx 2 century^{-1}$.

The present day model values of the local SFR and IFR surface density are $6.4 M_{\odot} pc^{-2} Gyr^{-1}$ and $3.3 M_{\odot} pc^{-2} Gyr^{-1}$ (lower panel in Fig. 8). For the last 8*Gyrs* the star formation rate varies very little. In general the local SFR is in good agreement with predictions from cosmologically motivated models for disc formation following in detail the mass aggregation history of dark matter halos similar to the one of the Milky Way (Firmani & Avila-Reese 2000; Hernández et al. 2001).

The absolute value of the star formation rate in the solar neighbourhood is very difficult to determine observationally and ranges from $2 - 10 M_{\odot} pc^{-2} Gyr^{-1}$ (Guesten & Mezger 1982). For the model star formation at the solar radius started ≈ 10 *Gyrs* ago. Observationally, Carraro et al. (1999) have determined a similar lower limit of the age of the galactic disc of $9 - 10$ *Gyrs* from the ages of open clusters. Binney et al. (2000) used *Hipparcos* observations of main-sequence and sub-giant stars determine the age of the solar neighbourhood to be 11.2 ± 0.75 *Gyr* with a lower limit of 9*Gyr*.

The ratio of the star formation rate to the mean star formation rate is easier to measure than the absolute star formation rate. According to the analysis by Binney et al. (2000) the star formation rate at the solar

neighbourhood has to have been very nearly constant (see also Haywood et al. 1997). Bertelli & Nasi (2001) found a star formation rate broadly increasing from past to the present time by comparing synthetic colour-magnitude diagrams to observation of field stars from the *Hipparcos* catalogue. Based on chromospheric activity in late type dwarfs Barry (1988) has found first evidence for a secular increase in the local star formation rate. Recent observations of the solar neighbourhood in deed favour a fluctuating history of the star formation rate with a slow secular increase. Observations of the star formation rate history by Rocha-Pinto et al. (2000a) based on the chromospheric age distribution of nearby stars are shown in Fig. 9. For comparison to our model we discarded all the stars that have observed ages older than the age of our model universe and rescaled the mean SFR accordingly (Helio Rocha-Pinto, private communication). Imagine that the oldest stars also have the largest errors in the age determination. The observed fluctuations on small time scales (0.5 *Gyrs*) over the recent 3*Gyrs* could have been triggered by the passage of spiral waves (Hernandez et al. 2000). Rocha-Pinto et al. (2000b) suggested close encounters with the the Magellanic clouds to account for the intermittent nature of the star formation rate and on scales of 1-3 *Gyrs*. The dashed line in Fig. 9 shows the predicted star formation rate history at the solar radius. To mimic the observational error we convolved the model data with an error of 0.1dex in age (solid line). It is obvious that our model can not reproduce the intermittent nature of the SFR as none of the possible physical origins are included. Globally, however, our model follows the observed trend for a secular increase in the SFR history very well.

In Fig. 10 we show the mean age of the stars versus radius at the present day. The mean stellar age of the disc is 5.4*Gyrs* in good agreement with the values of the thin disc of 5 – 7*Gyrs* (Robin et al. 2003) and the mean age of the stars at the solar neighbourhood is about 4*Gyrs*.

4.3 Metallicity evolution

Every successful model for the formation of the Milky Way has to be able to reproduce the metallicity distribution of stars at the solar neighbourhood. G and K dwarfs, with lifetimes comparable or longer than the age of the galactic disc, are good tracers of the star formation history and metal enrichment. It is now well established that there is a local dearth of low metallicity G- and, especially, lower mass K-stars, e.g. there are less low metallicity disc stars than predicted by simple closed box models for chemical evolution (van den Bergh 1962; Pagel & Patchett 1975; Tinsley 1980). In particular the distribution shows only a few stars at $[Fe/H] = -0.4$, rises steeply to a peak at $[Fe/H] \approx -0.1$ and falls off thereafter (Pagel & Patchett 1975; Beckman & Pagel 1989; Sommer-Larsen 1991; Rocha-Pinto & Maciel 1996; Jørgensen 2000; Nordström et al. 2004). Haywood (2001) proposed a revised version of the local metallicity distribution with the peak shifted to solar metallicity. Infall of low metallicity gas on long time scales has long been suggested as a possible solution for the 'G-dwarf problem' (Larson 1972; Lynden-Bell 1975; Pagel & Tautvaisiene 1995). As mentioned before the infall hypothesis is particularly inter-

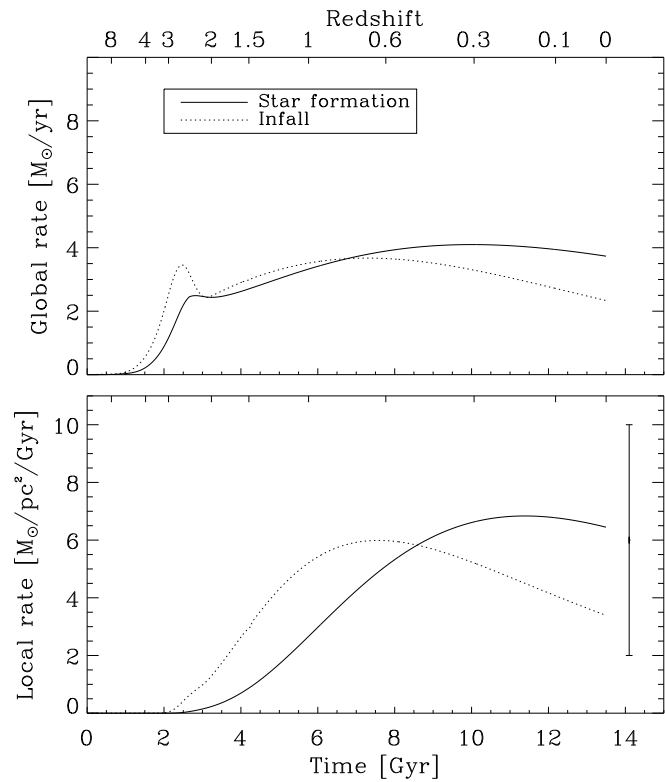


Figure 8. *Upper panel:* Evolution of the global star formation rate (solid) and the global infall rate (dotted). *Lower panel:* Local star formation rate (solid) and infall rate at the solar radius (dotted). The error bar indicates the observed range for the star formation rate (Guesten & Mezger 1982).

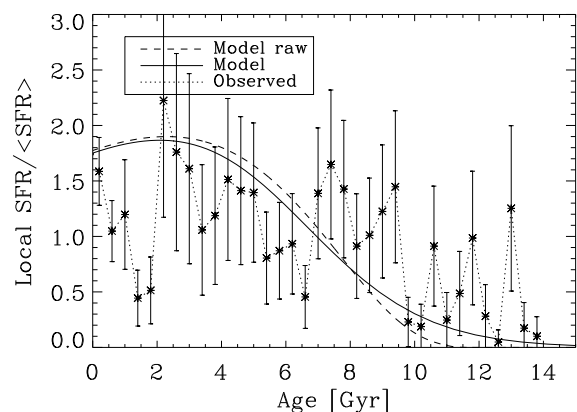


Figure 9. Ratio of star formation rate over mean star formation rate. The dashed line shows the raw model data, the solid line is the model data assuming an error in the age determination of 0.1 dex. The observed values with error bars are shown by the black symbols. Data from Rocha-Pinto et al. (2000a) have been kindly provided by Helio Rocha-Pinto.

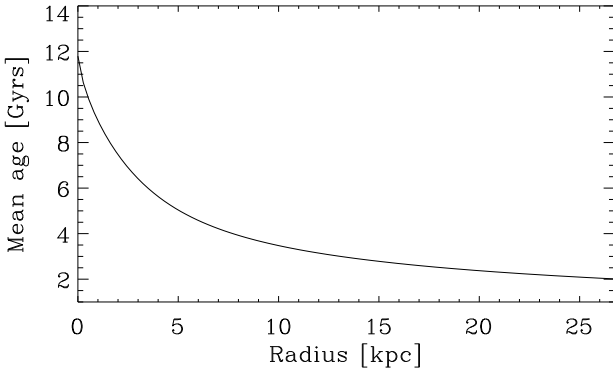


Figure 10. Mean age of the present day stellar disc versus radius. The mean age of the disc is 5.4 Gyrs, the mean age at the solar radius is 4 Gyrs.

esting as it offers a natural explanation for the existence of deuterium in the galactic disc which is destroyed by star formation (Ostriker & Tinsley 1975; Wakker et al. 1999). It has been suggested that the infall of high velocity clouds might continuously supply the galactic disc with metal poor gas. Recent observations have shown that the relatively high metallicities of HVC of about 0.1 solar rule out primordiality as well as a galactic origin (Sembach et al. 2004; Wakker et al. 2003).

To follow the metallicity evolution of our model galaxy we scaled the effective yield in Eqn. 36 to 0.1 dex below the solar value at the solar radius ≈ 4.5 Gyrs ago. Implicitly we assume that either the Sun has formed closer to the centre where the metallicity was slightly higher and moved outward thereafter probably due to orbital diffusion (Wielen 1977) or that the Sun had a slightly higher than typical metallicity representative of the ISM at the time of its formation. A further uncertainty is the exact chemical composition of the Sun. Recently Asplund et al. (2004) have derived the solar oxygen abundance using a 3D time-dependent hydrodynamical model of the solar atmosphere. Their value of $\log \epsilon_{\text{O}} = 8.66 \pm 0.05$ for the oxygen abundance and $Z = 0.0126$ for the solar metal mass fraction is significantly lower than the most commonly used value of $\log \epsilon_{\text{O}} = 8.93$ and, respectively, $Z = 0.0194$ derived by Anders & Grevesse (1989). The lower value for the solar metallicity is now in better agreement with the metallicity of the local ISM (Meyer et al. 1998; André et al. 2003), nearby B stars (Cunha & Lambert 1994; Kilian et al. 1994) and nearby young G and F dwarfs (Sofia & Meyer 2001).

We used the solar metallicity value of $Z_{\odot} = 0.0126$ to scale our model to 0.1 dex below the solar metallicity $Z = Z_{\odot} \times 10^{-0.1} = 0.01$ at solar radius 4.5 Gyrs ago, resulting in an effective yield of $Y = 0.0135$. The effective yield is significantly lower than in most previous studies as we used the revised lower solar metallicity value for normalisation. For the traditional value of $Z = 0.0196$ we would have needed an effective yield of $Y = 0.02$ if normalised to 0.1 dex below solar or $Y = 0.025$ if normalised to solar metallicity 4.5 Gyrs ago.

Fig. 11 shows the radial metallicity distribution of the ISM of the model disc. The distribution after 2, 4, 6, 8, 10, and 12 Gyrs is indicated by the dotted lines. For compar-

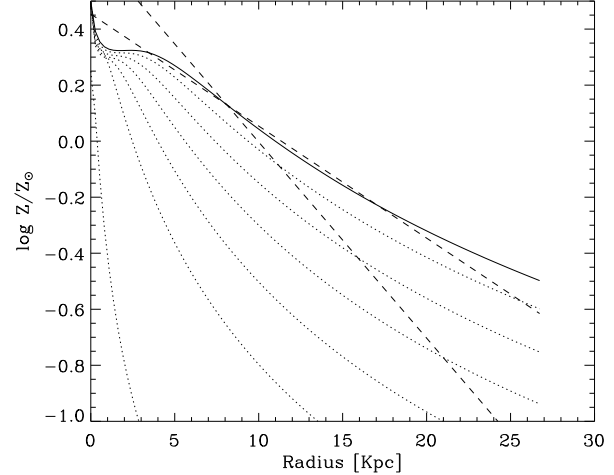


Figure 11. Radial metallicity distribution of the gas after 2, 4, 6, 8, 10, 12 and 13.6 Gyrs (thick solid line). The two dotted straight lines indicate a slope of $-0.07 \text{ dex kpc}^{-1}$ and $-0.04 \text{ dex kpc}^{-1}$. The metallicity gradient has been steeper in the past. The present day metallicity gradient of the stars is shown by the thick dot-dashed line.

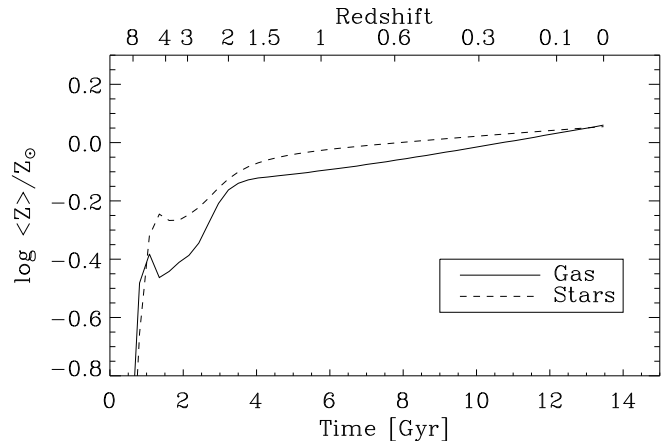


Figure 12. Time evolution of the mass weighted mean metallicity of the stars (dashed line) and the gas (solid line). After $z = 1.5$ the stellar metallicity does not show a strong evolution.

son we also show the present day metallicity gradient of the stars. At present time the metallicity gradient of the model is about $d \log(Z)/dr = 0.046 \text{ dex kpc}^{-1}$ at the solar radius. The metallicity gradient has been significantly steeper in the past (especially in the inner parts of the disc) which is a typical result for models using the inside-out formation scenario and has been proposed by several authors (Molla et al. 1997; Portinari & Chiosi 1999; Hou et al. 2000; Chiappini et al. 2001). Observationally, the existence of a gradient is well established. There is, however, considerable scatter in the published values (see e.g. Chiappini et al. (2001) for a discussion). Our model value is on the lower end of the observed abundance gradients of light elements, X , that are in the range of $-0.04 < d \log(X/H)/dr < -0.08 \text{ dex kpc}^{-1}$ (see e.g. Rolleston et al. (2000); Chiappini et al. (2001) and references therein). Recently Esteban et al. (2004) have de-

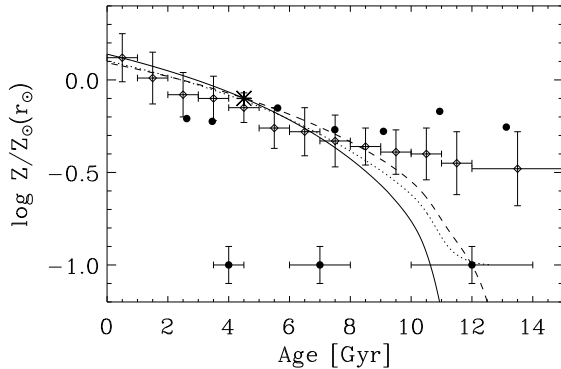


Figure 13. Age-metallicity distribution of the stars at the solar radius for infalling gas with metallicities $Z_{\text{IF}} = 1 \times 10^{-4}$ (dashed), $Z_{\text{IF}} = 0.1 Z_{\odot}$ (dotted) and $Z_{\text{IF}} = Z_{\odot}(0.3 \times 10^{-0.12z})$ (solid). The effective yield has been normalised to $\log(Z/Z_{\odot}) = -0.1$ 4.5Gyrs ago, indicated by the asterisk. Observations shown for comparison are Rocha-Pinto et al. (2000) - diamonds with error bars - and Nordström et al. (2004) - solid dots with typical errors shown in the lower part of the figure. Note that we did not fold the model data with the observational error in this case.

terminated the Oxygen gradient to $d \log(X/H)/dr < -0.044 \pm 0.010 \text{dex} \text{kpc}^{-1}$. In Fig. 12 we show the time evolution of the mass weighted mean metallicity of the stars and the gas at all radii where the total surface density is larger than $1 M_{\odot}/\text{pc}^2$. As we have continuous infall of low metallicity gas and the high metallicity gas is depleted at the center for most of the time the stellar metallicity is larger than the metallicity of the gas (see e.g. Akerman et al. 2004). After $z = 1$ the metallicity of the stars does not change significantly. The total mass of the stars, however, does increase by more than a factor of two (see Fig. 3).

The evolution of the metallicity of the ISM at the solar radius, which is equivalent to the age-metallicity distribution of the stars in the model, is shown in Fig. 13. We have computed the evolution for three different assumptions about the metallicity of the infalling gas Z_{IF} : (a) constant low metallicity not pre-enriched $Z_{\text{IF}} = 1 \times 10^{-4}$, (b) constant low metallicity enriched $Z_{\text{IF}} = 0.1 Z_{\odot}$ which is consistent with HVC and Ly α absorbers (Blitz et al. 1999), and (c) a time dependent metallicity taken from cosmological simulations, $Z_{\text{IF}} = 0.3 Z_{\odot} 10^{-0.12z}$, where z is the redshift (Cen & Ostriker 1999), assuming a present day metallicity of the infalling gas of $0.3 Z_{\odot}$. In general the late evolution is in good agreement with the age-metallicity distribution of Rocha-Pinto et al. (2000). For ages larger than 8Gyrs the models with pre-enriched infall are more consistent with observations. The age-metallicity relation published by Nordström et al. (2004) indicates an almost constant mean metallicity at all ages which might be a challenge to the model, especially for very old stars (for ages larger than 2.5Gyrs dots in Fig. 13). We note, however, that we have only plotted the raw distribution and did not take errors in the time nor in the metallicity determination into account.

In the upper panel of Fig. 14 we show the observed metallicity distribution of Rocha-Pinto & Maciel (1996), Jørgensen (2000), and Nordström et al. (2004). In general

the distributions peak at values of -0.2 to -0.1 and shows few or no stars below $[Fe/H] = -1$. The dotted thin lines in the lower panel of Fig. 14 show the raw metallicity distributions of the model galaxy, binned according to observations, for the three different metallicities of the infalling gas. The distributions are very similar and there is a very good agreement between the theoretical and the most recently observed distributions (see also Karatas et al. 2005). Therefore pre-enrichment does not influence the local metallicity distribution in our model. The constant gas infall over almost 10Gyrs determines the shape of the distribution. For a better comparison to the observed distributions we folded the average model data with a Gaussian with a dispersion of 0.15 dex, which is typical for observations by Rocha-Pinto & Maciel (1996), an error of 0.1 dex would be more typical for the Nordström et al. (2004) data. The resulting distributions are shown by the solid and dashed lines in the lower panel of Fig. 14. Independent of the assumed error there is a very good agreement with observations of the distribution of $[Fe/H]$. Haywood (2001) has proposed a revision of the metallicity distribution resulting in a shift of the peak value to $[Fe/H] = 0$ (shown as a mass fraction in the lower panel of Fig. 14).

4.4 Photometric evolution

We use the metal dependent models for the spectral evolution of stellar populations of Bruzual & Charlot (2003), kindly provided by the authors, assuming a Salpeter IMF to compute the photometric properties of our model galaxy.

Fig.15 shows the time evolution of the absolute magnitudes, the total luminosities and the colours of the model galaxy at different wavelengths. The total luminosities were calculated assuming absolute magnitudes for the Sun of $[K, H, R, V, B, U] = [3.28, 3.32, 4.42, 4.83, 5.48, 5.61]$ (Binney & Merrifield 1998). The absolute U and B magnitudes stay relatively constant after 6Gyrs reflecting the almost constant global star formation rate (Fig. 8). At longer wavelengths the luminosity is slowly increasing due to the mass assembly in the disc. The H-band magnitude of $M_H = -23.0$ ($L_H = 3.5 \times 10^{10} L_{\odot, H}$) is in excellent agreement with the value expected from the H-Band Tully-Fisher relation of $M_H = -22.84$ assuming $v_c = 210 \text{km s}^{-1}$ (Pierce & Tully 1992). A direct comparison to the luminosity of the Milky Way is more complicated as the photometrical determination of the total luminosity of the Galaxy is very difficult. As a possible range Binney & Merrifield (1998) refer to observed values of $L_K = 4.9 \times 10^{10} L_{\odot, K}$ (Kent et al. 1991), which is close to the model value of $L_K = 4.1 \times 10^{10} L_{\odot, K}$, and $L_L = 2.2 \times 10^{10} L_{\odot, L}$ (Freudenreich 1998). The values have been corrected using the solar magnitudes given above (see Binney & Merrifield 1998). The absolute V-band luminosity of the model is $L_V = 1.9 \times 10^{10} L_{\odot, V}$ which is within the observed range of $1.4 \times 10^{10} < L_V < 2.1 \times 10^{10} L_{\odot, V}$ by van der Kruit (1986) and slightly higher than the observed unobscured value of $L_V = 1.25 \times 10^{10} L_{\odot, V}$ ($M_V = -20.4$) (Bahcall & Soneira 1980). Note that uncertain dust corrections are important in fixing the observed value. The surface brightness profiles at different wavelengths are shown in the upper panel of Fig. 16. Two observed values in the K- and B-band at the solar radius are overplotted (Binney & Merrifield 1998). The middle panel shows the

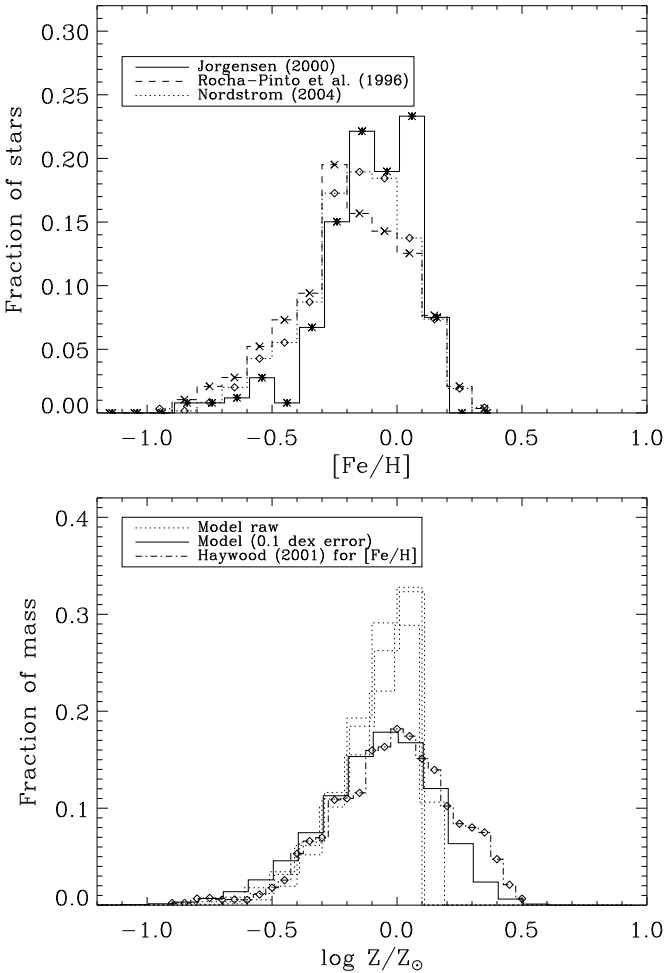


Figure 14. *Upper panel:* Observed metallicity distributions of Rocha-Pinto & Maciel (1996) (dashed), Jørgensen (2000) (solid) and Nordström et al. (2004) (dotted). *Lower panel:* The thin dotted lines show the (almost identical) binned mean raw metallicity distribution of model galaxy for the models with the three different infall metallicities (See Fig. 13). The solid line shows the average binned model distribution assuming an error of 0.15 dex in the metallicity determination.

corresponding luminosity density profiles using the solar magnitudes given above. All profiles are exponential in the outer parts and flatten out towards the centre. The present day colour profiles are shown in the lower panel of Fig. 16. The galaxy get redder at the centre which is a combined effect of increasing metallicities (Fig. 11) and increasing stellar ages towards the centre (see Fig. 10). The $B - V$ colour at the solar radius is $B - V = 0.4$ as opposed to an observed value of $B - V = 0.6 - 0.8$ (Boissier & Prantzos 1999). The $B - K$ colour of $B - K = 3.0$ is more similar to observations of $B - K = 3.13$ (Binney & Merrifield 1998). Over all the model galaxy seems to be slightly bluer than the Milky Way. This might be due to uncertain dust corrections. Additionally, the blue luminosity is very sensitive to the very recent (1Gyr) star formation history. As we have seen from observations (Fig. 9) the recent star formation rate has been below average. This effect alone can account for the difference in the blue luminosity of the model and the Milky Way.

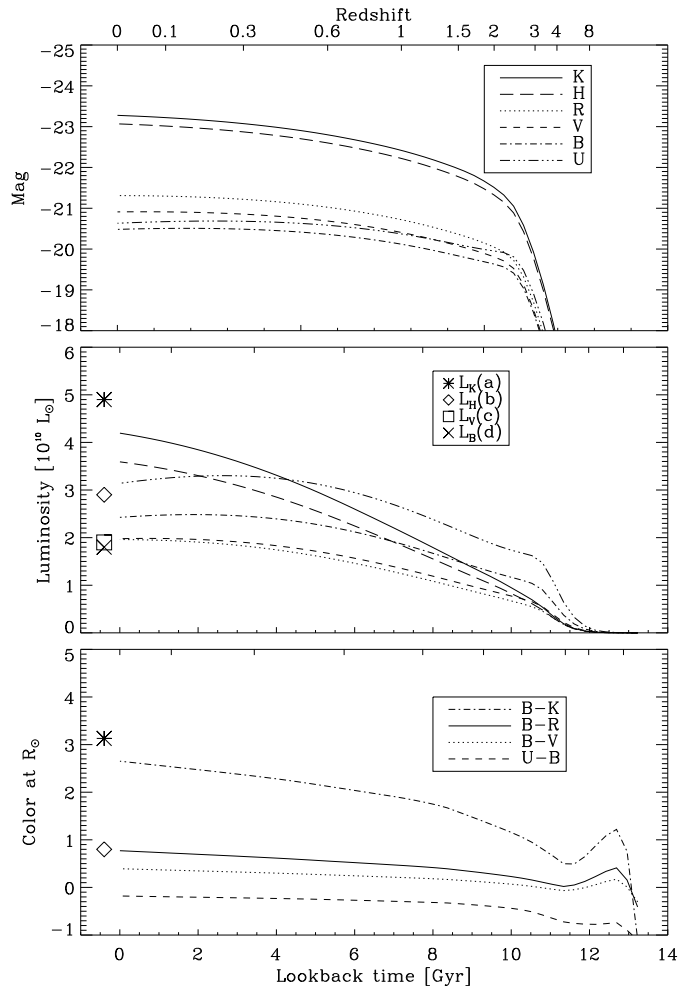


Figure 15. *Upper panel:* Absolute magnitude of the model galaxy versus time. *Middle panel:* Evolution of the total luminosities with time. Observed values are from: (a) Kent et al. (1991) , (b) Pierce & Tully (1992), (c) Bahcall & Soneira (1980), (d) van der Kruit (1986).

To calculate the scale lengths in the different bands we have fitted an exponential in the range of $1.5 < r_d < 3.0$ scale lengths of the total surface density distribution. The scale lengths increase to shorter wavelengths (Fig. 17). This effect is weaker at earlier times. At present the B-band scale length $r_{d,B} = 3.7\text{kpc}$ is a factor of ≈ 1.2 larger than the K-band scale length $r_{d,K} = 3.0\text{kpc}$. This trend is observed and is in good agreement with other Milky Way type spiral galaxies. de Jong (1996) investigated a sample of 86 nearly face-on spiral galaxies and concluded that spiral galaxies of the same type as the Milky Way have disc scale lengths that are a factor of 1.25 ± 0.25 larger in the B-band than in the K-band. This effect reflects the over all inside out formation process for disc galaxies and has been found in similar studies (Boissier & Prantzos (1999) have found $r_{d,B}/r_{d,K} = 1.5$ which is also in good agreement).

In Fig 18 we show the time evolution of the K-, V-, and B-band surface brightness. The discs had steeper profiles and higher values for the central surface brightness in the past. This is in good agreement with recent observations of

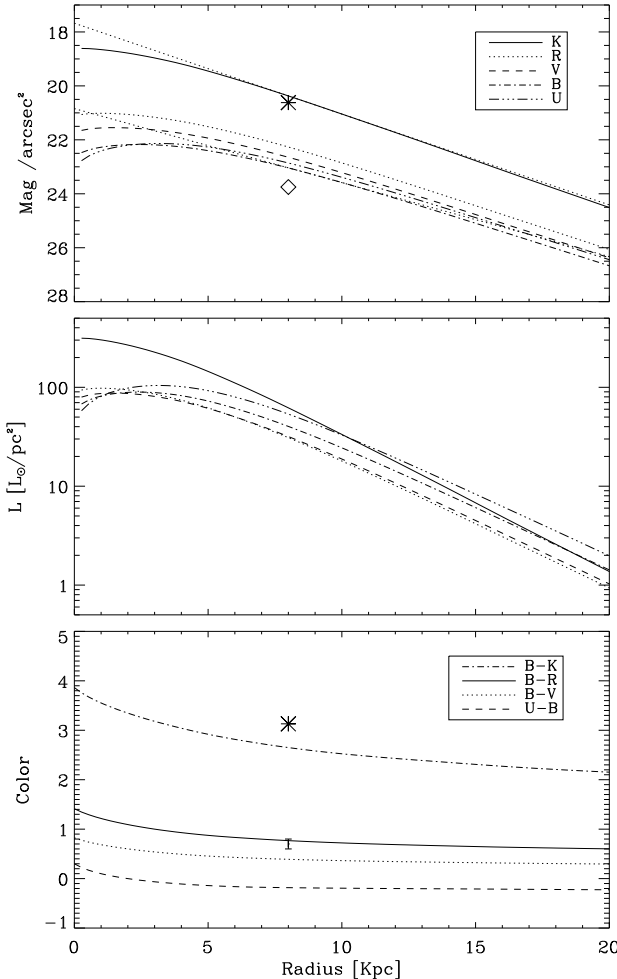


Figure 16. Photometric properties versus radius. Observed values are $\mu_K = 20.62$ (star) and $\mu_B = 23.75$ (diamond) (Binney & Merrifield 1998) The observed colors are $B - K = 3.13$ (Binney & Merrifield 1998) indicated by the star in the lowest panel and $0.6 < B - V < 0.8$ (see Boissier & Prantzos 1999) indicated by the error bar.

disc evolution with redshift that favour the inside-out disc formation process (Barden et al. 2005).

Given the luminosity distributions we can compute the variation of the mass-to-light ratio at different wavelengths versus radius (Fig. 19). In the K-band the value at the solar neighbourhood is close to 0.8 if we include the mass of the gas and the stars. Assuming a column density of dark matter within 0.5kpc of $11M_\odot\text{pc}^2$ the K-band mass-to-light ratio would be around in agreement with the observed value Binney & Merrifield (1998). However, the observed value is uncertain as the quantities used to calculate the mass-to-light ratio itself have already large errors.

5 THE EFFECT OF A DIFFERENT IMF

In this section we investigate the effect of a different IMF on the properties of our model disc galaxy. We tested the Chabrier (2003) IMF which provides a better fit to low mass stars and brown dwarfs in the Milky Way using the

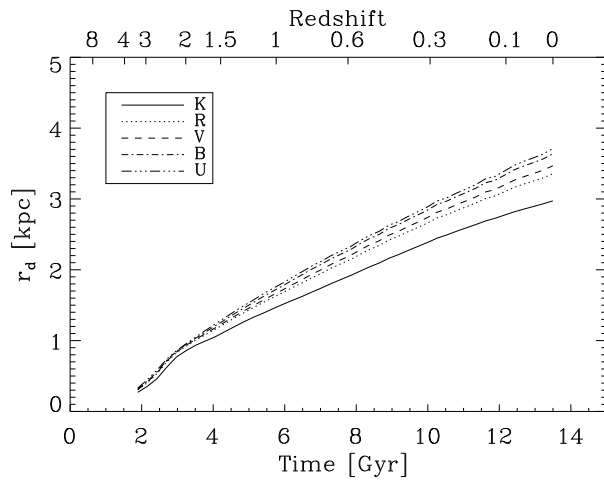


Figure 17. Exponential scale lengths of the surface brightness distribution measured at the different wavelengths versus time. At shorter wavelengths the disc has a larger scale length.

corresponding evolutionary models of Bruzual & Charlot (2003). For the Chabrier IMF the fraction of gas returned to the ISM by evolved stars is higher than for the Salpeter IMF (Bruzual & Charlot 2003). Therefore we have changed the parameters in Eqn. 35 to $R_* = 0.44$, $\delta_* = 1.5$, and $\tau_0 = 1 \times 10^8$ to fit the corresponding return fractions of Bruzual & Charlot (2003). We have run the model using the Chabrier IMF with exactly the same input parameters except the effective yield. It has been reduced to $Y = 0.013$ to guarantee a metallicity of 0.1 dex below the solar value at the solar radius $\approx 4.5\text{Gyrs}$ ago. We have summarized the comparison in Figs. 20 and 21. The total gas mass and the local gas surface density are about 20% higher due to the higher gas return fraction of the Chabrier IMF (two upper panels in Fig. 20). The stellar masses are reduced by the corresponding amount. Similarly the present day local star formation rate is about 20% higher (third panel in Fig. 20) and the mean age of the stars at the solar neighborhood is reduced to 3.8Gyrs . The effect on the luminosities is stronger as the Chabrier IMF in general leads to 1.4 - 1.8 times smaller mass-to-light ratios than the Salpeter IMF (Chabrier 2003; Bruzual & Charlot 2003), e.g. the K-band luminosity increases from $L_K = 4.1 \times 10^{10} L_{K\odot}$ to $L_K = 7.2 \times 10^{10} L_{K\odot}$ (fourth panel in Fig. 20). The lowest panel in Fig. 20 shows the time evolution of the local colors that are only weakly effected by the different IMF as already mentioned by Bruzual & Charlot (2003).

In the upper panel of Fig. 21 we show a comparison between the radial metallicity distribution of the ISM for a Salpeter and a Chabrier IMF. The Chabrier IMF leads to a higher metallicity at the central region and the present day gradient at the solar radius is increased to $-0.056\text{dex kpc}^{-1}$. The Chabrier IMF results in a larger fraction of stars with super solar metallicity at the solar radius but the shape of the metallicity distribution at the solar radius remains basically unchanged (lower panel in Fig. 21).

Taking the observational errors into account the properties of the model using a Chabrier IMF are as well in agreement with observations, especially the metallicity gradient

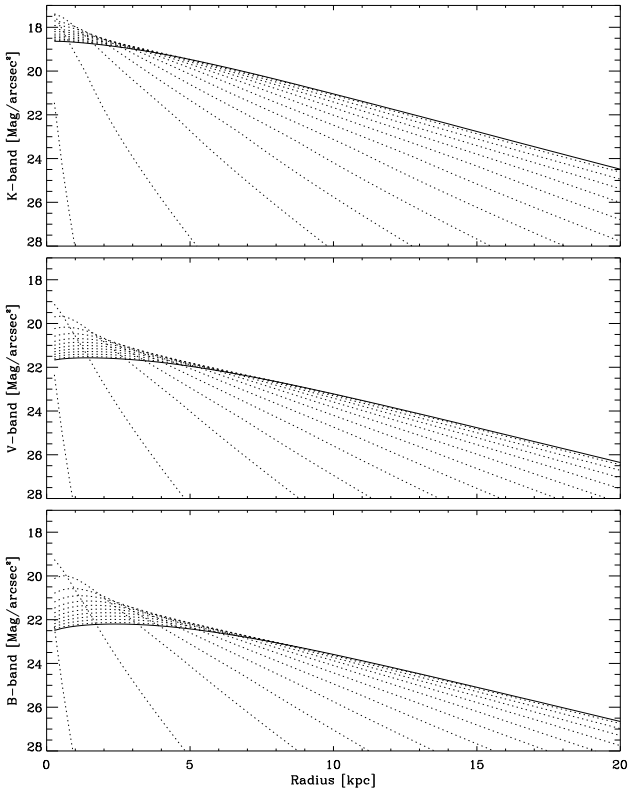


Figure 18. Evolution of the K-, V-, and B-band rest frame surface brightness profiles with time. The dashed line from the left to the right show the surface brightness profiles from early times to now. The profiles are plotted every $1.4Gyrs$. The present day profiles is the solid line (see Fig. 16).

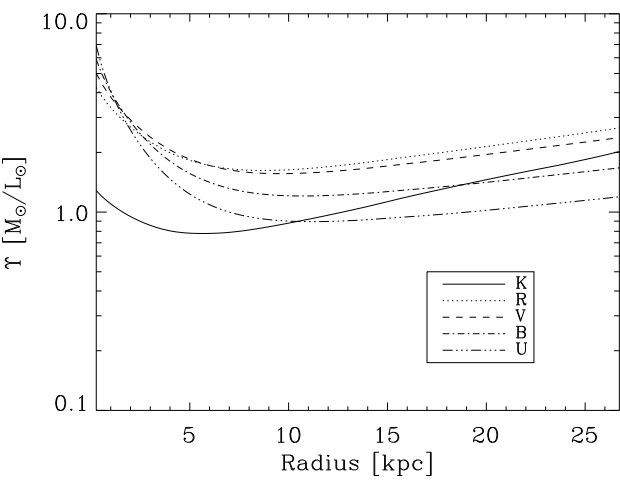


Figure 19. Present day disc mass-to-light ratio (stellar + gaseous mass, the exact dark matter contribution is unknown) versus radius at different bands. Dark matter is not included here as the exact distribution is unknown. Assuming a column density of dark matter within $0.5kpc$ of $11M_⊙pc^2$ at the solar radius the K- and B-band mass-to-light ratios would be 1 and 1.6, respectively.

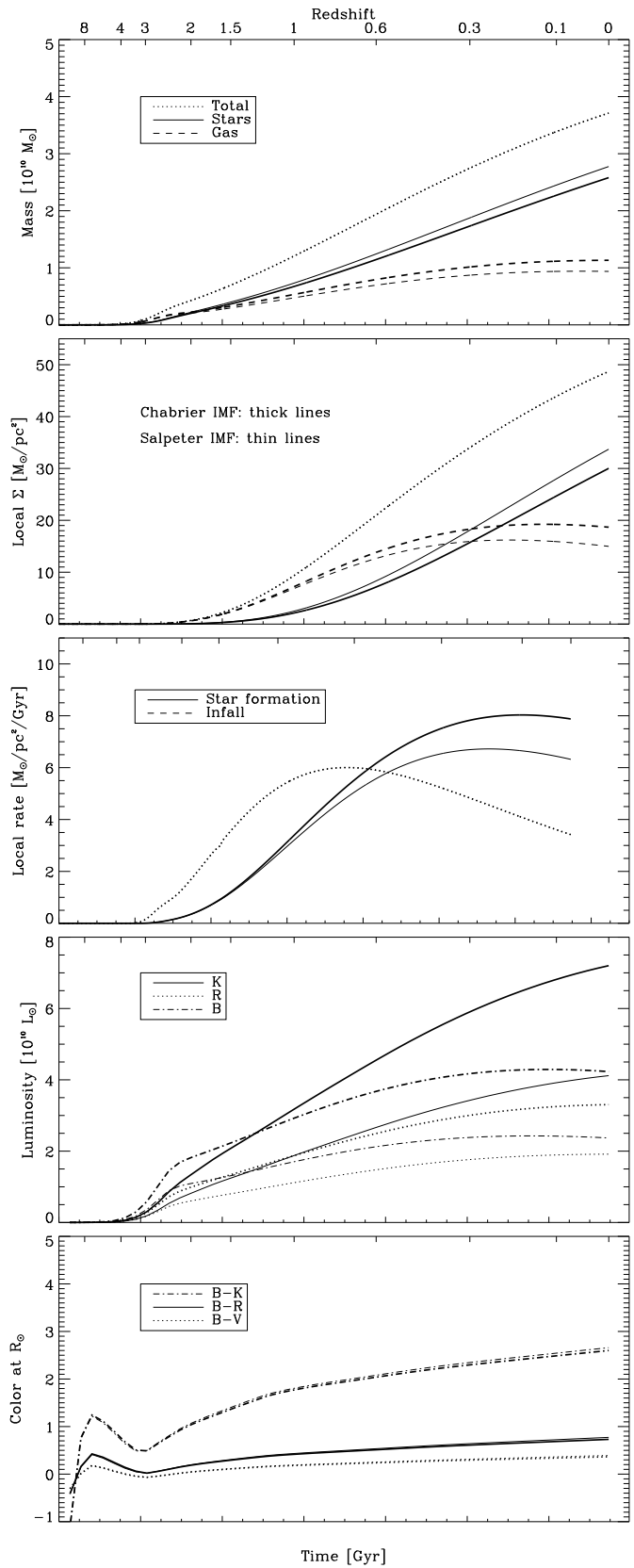


Figure 20. Comparison of the time evolution of already introduced characteristic model parameters for a Salpeter IMF (thin lines) and a Chabrier IMF (thick lines).

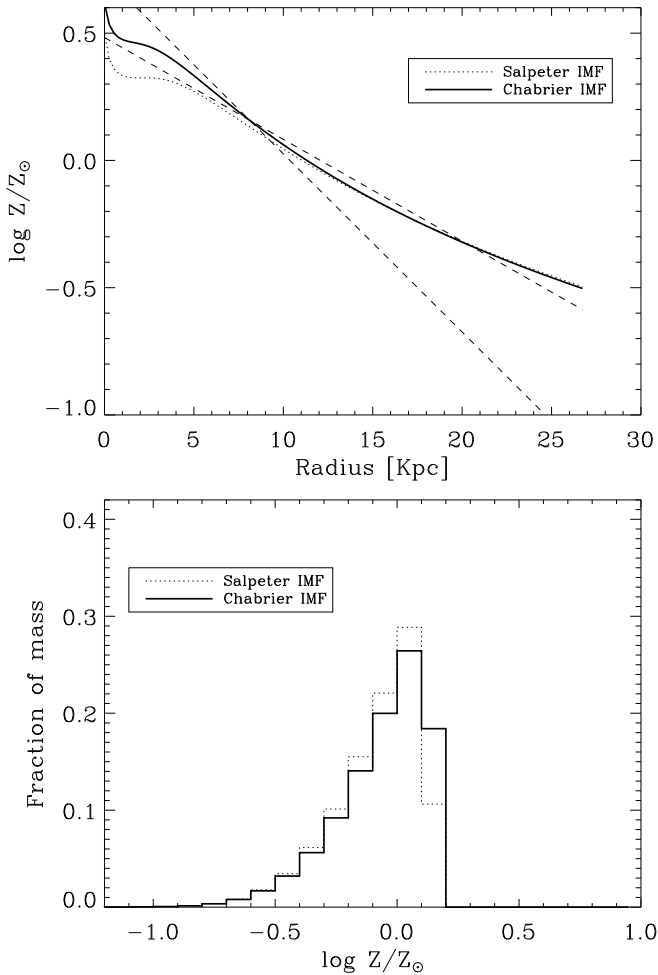


Figure 21. *Upper panel:* Present day radial metallicity distribution of the gas for the Salpeter IMF (thin dotted line) and the Chabrier IMF (thick solid line). The two dotted straight lines indicate a slope of $-0.07 \text{dex kpc}^{-1}$ and $-0.04 \text{dex kpc}^{-1}$. *Lower panel:* Local metallicity distribution of the stars for the Salpeter IMF (thin dotted line) and the Chabrier IMF (thick solid line).

and the local metallicity distribution. The local value of the gas surface density might be at the upper limit of observations (the gas distribution at the solar radius is very difficult to measure) but could be reduced by assuming a higher star formation efficiency. Therefore we can not conclude that either the Salpeter IMF or the Chabrier IMF leads to model properties that are over all in better agreement with observations.

6 THE EFFECT OF STAR FORMATION THRESHOLDS

Martin & Kennicutt (2001) have shown that disc galaxies show prominent breaks in their outer $H\alpha$ profiles giving evidence for the existence of a critical surface density beyond which the star formation is strongly suppressed. A possible consequence of a star formation threshold density could be the observed truncation or outer breaks in the profile of stellar discs (van der Kruit 1979; de Grijs et al. 2001). However,

other possible explanations, e.g. truncation by the maximum angular momentum of the protogalaxy (van der Kruit 1987), have been given as well. As we have seen in Section 2 there is observational evidence that the stellar disc of the Milky Way is truncated at a radius of $\approx 15 \text{kpc}$. In this section we investigate whether this truncation can be caused by a threshold gas surface density for star formation.

Based on observational constraints any star formation law for disc galaxies will break down at gas surface densities of

$$\Sigma_{\text{crit}} < 5 - 10 M_\odot \text{pc}^{-2}, \quad (37)$$

where the star formation is in general strongly suppressed (Kennicutt 1998). However, in individual cases the actual threshold value may vary by an order of magnitude (Martin & Kennicutt 2001) and the simple prescription is not valid. It has been argued for a long time that gravitational instabilities could determine the threshold density for star formation (Toomre 1964; Quirk 1972; Kennicutt 1989) by coriolis forces

$$\Sigma_{\text{crit}} = \alpha_Q \frac{\sigma_{\text{gas}} \kappa}{\pi G} \quad (38)$$

where σ_{gas} is the velocity dispersion of the gas, κ is the epicyclic frequency,

$$\kappa^2(r) = 2 \left(\frac{v^2}{r^2} + \frac{v}{r} \frac{dv}{dr} \right), \quad (39)$$

and $\alpha_Q \equiv 1/Q$ defines an effective Toomre stability parameter. Martin & Kennicutt (2001) favour a value of $\alpha_Q = 0.69$ corresponding to $Q = 1.45$ for their sample. Numerical studies of self-gravitating gas discs indicate values up to $Q = 1.6$ (Kim & Ostriker 2001; Kim et al. 2003). Alternatively, the disc can be stabilised by shear forces

$$\Sigma_{\text{crit}} = \alpha_A \frac{\sigma_{\text{gas}} A}{\pi G}, \quad (40)$$

where A is the Oort constant (Hunter et al. 1998). For constant circular velocities v_c like in the outer parts of disc galaxies both criteria reduce to

$$\Sigma_{\text{crit}} = \alpha_Q \frac{\sqrt{2} \sigma_{\text{gas}} v_c}{\pi G r} = \alpha_A \frac{\sigma_{\text{gas}} v_c}{2 \pi G r} \quad (41)$$

and $\alpha_Q = \alpha_A / (2\sqrt{2})$. Both criteria differ in the innermost part of the disc if the circular velocity is not constant.

The above criteria only consider the theoretical case of a purely gaseous disc. In real galaxies the stellar component can have a destabilising effect on the gas. Wang & Silk (1994) derived an effective stability parameter α_{eff} taking the stellar surface density Σ_* and velocity dispersion σ_* into account

$$\Sigma_{\text{crit}} = \alpha_{\text{eff}} \frac{\sigma \kappa}{\pi G}, \text{ where } \alpha_{\text{eff}} = \left(1 + \frac{\Sigma_* \sigma_{\text{gas}}}{\Sigma_{\text{gas}} \sigma_*} \right)^{-1}. \quad (42)$$

They have successfully applied their criterion to the Milky Way, which has recently been confirmed by Boissier et al. (2003).

We have tested the influence of the threshold prescriptions given by Eqns. 37, 41, and 42 on the evolution of the outer parts of our model disc. For the constant threshold case (Eqn. 37) we assumed a critical gas density of $\Sigma_{\text{crit}} = 7 M_\odot \text{pc}^{-2}$, for the Toomre based criterion (Eqn. 41)

we used the observed value of $\alpha_Q = 0.69$ and a velocity dispersion of the gas of $\sigma_{\text{gas}} = 6 \text{ km s}^{-1}$. For the third version we assumed a stellar velocity dispersion based on $Q = 1.6$ to compute α_{eff} . We mimicked the fluctuating nature of the gas surface density at a given radius by randomly drawing a surface density from a Gaussian with a mean of the model surface density and a dispersion of 10% that is compared to the threshold value. This procedure guarantees that some star formation can occur even in regions where the mean surface density is below threshold. As soon as the gas density drops below the critical density we let the star formation rate cease immediately

$$\Sigma_{\text{SFR}}(r, t) = 0 \text{ for } \Sigma_{\text{gas}} < \Sigma_{\text{crit}}. \quad (43)$$

We focus on effects on the outer disc at radii larger than 7 kpc . In the central parts a simple threshold prescription is less meaningful due to the limitations of some of the prescriptions (see above) and the uncertain influence of a central bulge or bar component which is not explicitly included in our model. The effect of the cutoff on the outer mass, gas and the K-band light distribution is shown in Fig. 22. At radii smaller than $\approx 12 \text{ kpc}$, the cutoff has almost no effect. At radii of about 12 – 13 kpc the cutoff models produce a sharp decline in the stellar distribution in agreement with observations of the Milky Way and external disc galaxies. The effect on the K-band light profile is shown in the lowest panel of Fig. 22. All models produce a similar behaviour. The gas surface density is slightly increased compared to the model without threshold at radii larger than 12 kpc and is qualitatively in better agreement with observations. Other physical mechanisms might be important for disc truncations as well (see e.g. Schaye 2004). However, based on this model we conclude that even a simple recipe for star formation cutoff can be successfully implemented in analytical models and producing truncated present day stellar discs in good agreement with observations. Qualitatively our results are in agreement with previous models by Chiappini et al. (1997, 2001) who used fixed threshold value. At the solar neighbourhood a cutoff leads to a delayed onset of star formation (Fig. 23). For all models the star formation sets in after ≈ 5 – 6 Gyr .

7 SUMMARY & CONCLUSION

We have presented a simple model for the evolution of the Milky Way in a cosmological context. We start with the current observed gross properties of the Galaxy. Assuming simple scaling relations derived from the standard properties of a concordance Λ CDM cosmological model that determine the time evolution of the infall rate onto the galaxy and also the time dependence of the rotation curve we have our back-bound state. We supplement this with a standard star formation prescription, and chemical evolution models assuming a Salpeter IMF and are able to reproduce a large number of observed global and local properties of the Milky Way to a similar accuracy as previous successful models for chemical evolution and chemo-spectrophotometric models (e.g. Chiappini et al. 1997; Prantzos & Silk 1998 and references therin). However, in contrast to most previous models the evolution of the infall rate itself with time and radius is not a free parameter in the model presented here.

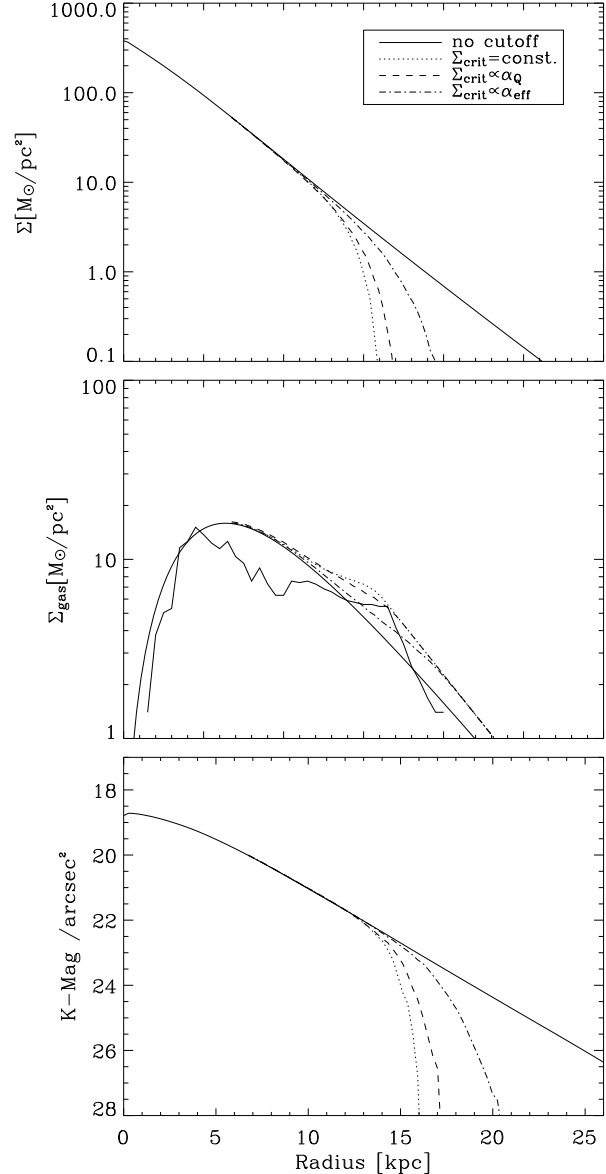


Figure 22. The stellar surface density (upper panel), the gas surface density (middle panel) and the K-band light distribution (lower panel) without star formation cutoff (solid line) and with cutoff for three different prescriptions for the critical surface density: constant at $7 M_{\odot} \text{ pc}^{-2}$ (dotted), based on the instability of the gas disc (dashed) and based on the instability of the combined stellar and gaseous disc (dashed-dotted).

Globally, the gas infall rate and the star formation rate are almost constant with time at ≈ 2 – $4 M_{\odot} \text{ yr}^{-1}$ during the evolution of the disc. The total mass of the present day model galaxy in stars and in gas is $2.7 \times 10^{10} M_{\odot}$ and $9.5 \times 10^9 M_{\odot}$, respectively, and the disc has an absolute K-band magnitude of -23.2 . The present day scale length at longer wavelengths is shorter than at shorter wavelengths. The mean age of long lived stars at the solar neighbourhood is about 4 Gyr . Presently, the local surface density of the stars and gas are 35 and $15 M_{\odot} \text{ pc}^{-2}$, respectively. We have been able to reproduce a narrow metallicity distribution of the stars at the solar radius with a peak at

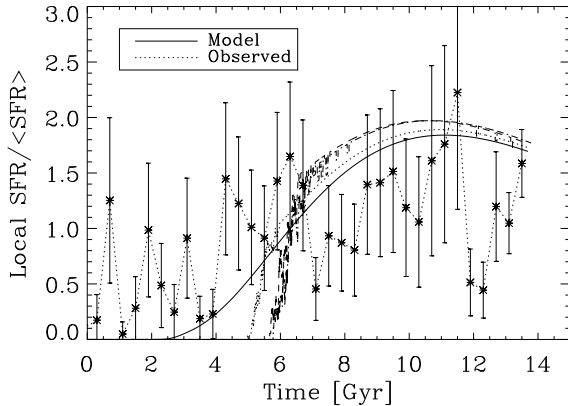


Figure 23. Star formation history at the solar neighbourhood for different models of cutoff. In general, star formation cutoff leads to a later onset of star formation and a slightly younger age of the solar neighbourhood. (see Fig. 9)

$[Z/Z_{\odot}] = -0.1$ and a radial gradient of $-0.046dexkpc^{-1}$ which has been significantly steeper in the past. We have tested different threshold density prescriptions for star formation that all lead to a truncation of the stellar disc at about $12kpc$. Changing the IMF from Salpeter to Chabrier leads to an increased gas content and higher luminosities of the model galaxy. The present day metallicity gradient is steeper and the local metallicity distribution is only weakly affected. Based on our results we can not decide whether a Chabrier IMF or a Salpeter IMF leads to a better agreement with observations. In total we have been able to produce well the local age and metallicity distributions and the star formation history which provide the local fossil record of our Galaxies' evolution.

The model described here is, of course, over simplified. Several physical processes that are likely to play a role during the formation of disc galaxies have been excluded. In the following we mention only a few processes that might have an influence on the over all results: In the hierarchical framework, disc galaxies do not only grow continuously by smooth accretion of gas but also in discrete steps by minor mergers and accretion of small satellites. Simulations of disc galaxy formation have shown that not only gas is building up the disc but a small amount (up to 10%) of old stars that have formed within small satellites are continuously added to the disc by accretion (Abadi et al. 2003b; Meza et al. 2004). A process that is presently observed in our Milky Way for the Sagittarius dwarf galaxy and other small satellites (e.g. Ibata et al. 1997; Newberg et al. 2002; Martin et al. 2004; Helmi et al. 2005). Accretion of satellites might add very old stars to the solar neighbourhood thereby increasing its apparent age. The smooth accretion as assumed in the model can only be seen as an approximate representation of the past integrated accretion rate. In real disc galaxies minor mergers, satellite encounters and the passage of spiral waves might locally enhance the star formation rate and lead to the intermittent star formation history that is observed in the local neighbourhood (Rocha-Pinto et al.

2000a; Hernandez et al. 2000). This oscillatory behaviour can not be reproduced by the model. In particular, we have not been able to exactly fit the observed colours at the solar neighbourhood. We have tested oscillatory star formation rates with a local depression at the solar neighbourhood about 1 Gyr ago and found a good agreement with the data. The present day local and global colour of discs can not strongly constrain any simple and generally valid model on disc galaxy evolution. In particular, the influence of an oscillatory star formation history on the metallicity evolution is very small as the metallicity is basically determined by the past integrated star formation history (see also Hirashita et al. 2001).

In this paper we have focused on the evolution of the disc component only and did not include explicitly the effect of gas infall from a stellar spheroidal component (halo) of the Milky Way. This process, that has been investigated by several authors, has been proposed (see e.g. Ostriker & Thuan 1975; Rana 1991; Wyse & Gilmore 1992) as a possible solution to the G-dwarf problem as it would provide pre-enriched gas from halo stars. Implicitly, we have investigated this effect by allowing the metallicity of the infalling (to the disc) gas to have the metallicity expected from gas pre-processed through halo stars and the gas expelled from nearby dwarf systems. The present metallicity distribution at the solar neighbourhood is determined by the almost constant gas infall rate over the last $10Gyrs$ is only very weakly effected by pre-enrichment. We will focus on the role of bulge components in the framework of our model in a subsequent paper.

The influence of radial gas flows possibly triggered by tidal interactions, infalling low angular momentum gas or viscosity in the gas disc have been investigated by several authors (see e.g. Portinari & Chiosi (2000) and references therein). If important inflowing gas is likely to increase the metallicity gradient and steepen the density profile. On the other hand orbital diffusion of stars might flatten the gradient again. In addition, we assumed instantaneous mixing of recycled material within one ring and avoided complicated feedback and mixing processes that might be more or less important in the early or late phases of the disc evolution (see e.g. Efstathiou 2000)

All the above processes might play a role during disc galaxy evolution but were not implicitly included in the model. Still the presented results look very promising. We might conclude that to first order smooth gas infall followed by local star formation as a function of the local gas density is the dominant process shaping the Milky Way and other disc galaxies.

In this paper we have taken an archaeological approach to galaxy evolution - to check if the computed history is consistent with the local fossil record. Alternatively, one can compare the evolution directly with the past history as seen in for instance in the HDF or HUDF or redshift surveys like GEMs. We will pertain to this test in a subsequent paper but simply note that the evidence is consistent with an inside-out formation scenario of discs, e.g. smaller average discs sizes at earlier times. Recent high redshift observations strongly support this scenario Ravindranath et al. 2004; Ferguson et al. 2004; Barden et al. 2005; Trujillo et al. 2005).

ACKNOWLEDGMENTS

The authors thank Thomas Dame, Helio Rocha-Pinto and Johan Holmberg for kindly providing their observational data and useful suggestions. We also thank Gerard Gilmore, Rob Kennicutt, Scott Tremaine and Max Pettini for many valuable comments on the manuscript. We also thank the anonymous referee for valuable comments.

REFERENCES

Abadi M. G., Navarro J. F., Steinmetz M., Eke V. R., 2003a, *ApJ*, 591, 499

Abadi M. G., Navarro J. F., Steinmetz M., Eke V. R., 2003b, *ApJ*, 597, 21

Akerman C. J., Carigi L., Nissen P. E., Pettini M., Asplund M., 2004, *A&A*, 414, 931

Allen C., Carigi L., Peimbert M., 1998, *ApJ*, 494, 247

Anders E., Grevesse N., 1989, *Geochim. Cosmochim. Acta*, 53, 197

André M. K., Oliveira C. M., Howk J. C., Ferlet R., Désert J.-M., Hébrard G., Lacour S., Lecavelier des Étangs A., Vidal-Madjar A., Moos H. W., 2003, *ApJ*, 591, 1000

Asplund M., Grevesse N., Sauval A. J., Allende Prieto C., Kiselman D., 2004, *A&A*, 417, 751

Bahcall J. N., Flynn C., Gould A., 1992, *ApJ*, 389, 234

Bahcall J. N., Soneira R. M., 1980, *ApJS*, 44, 73

Barden M., Rix H., Somerville R. S., Bell E. F., Haeusler B., Peng C. Y., Borch A., Beckwith S. V. W., Caldwell J. A. R., Heymans C., Jahnke K., Jogee S., McIntosh D. H., Meisenheimer K., Sanchez S. F., Wisotzki L., Wolf C., 2005, ArXiv Astrophysics e-prints

Barry D. C., 1988, *ApJ*, 334, 436

Beckman J. E., Pagel B. E., 1989, *Ap&SS*, 156

Bertelli G., Nasi E., 2001, *AJ*, 121, 1013

Bertschinger E., 1985, *ApJS*, 58, 39

Binney J., Dehnen W., Bertelli G., 2000, *MNRAS*, 318, 658

Binney J., Merrifield M., 1998, *Galactic astronomy. Galactic astronomy / James Binney and Michael Merrifield.* Princeton, NJ : Princeton University Press, 1998. (Princeton series in astrophysics) QB857 .B522 1998 (\$35.00)

Binney J. J., Evans N. W., 2001, *MNRAS*, 327, L27

Blitz L., Spergel D. N., Teuben P. J., Hartmann D., Burton W. B., 1999, *ApJ*, 514, 818

Boissier S., Prantzos N., 1999, *MNRAS*, 307, 857

Boissier S., Prantzos N., 2000, *MNRAS*, 312, 398

Boissier S., Prantzos N., Boselli A., Gavazzi G., 2003, *MNRAS*, 346, 1215

Bottema R., 1993, *A&A*, 275, 16

Braun R., Thilker D. A., 2004, *A&A*, 417, 421

Bruzual G., Charlot S., 2003, *MNRAS*, 344, 1000

Cappellaro E., Turatto M., Benetti S., Tsvetkov D. Y., Barutunov O. S., Makarova I. N., 1993, *A&A*, 273, 383

Carraro G., Girardi L., Chiosi C., 1999, *MNRAS*, 309, 430

Casuso E., Beckman J. E., 2004, *A&A*, 419, 181

Cen R., Ostriker J. P., 1999, *ApJ*, 519, L109

Chabrier G., 2003, *PASP*, 115, 763

Chang R., Shu C., Hou J., 2002, *Chinese Journal of Astronomy and Astrophysics*, 2, 226

Chang R. X., Hou J. L., Shu C. G., Fu C. Q., 1999, *A&A*, 350, 38

Chiappini C., Matteucci F., Gratton R., 1997, *ApJ*, 477, 765

Chiappini C., Matteucci F., Romano D., 2001, *ApJ*, 554, 1044

Chiappini C., Renda A., Matteucci F., 2002, *A&A*, 395, 789

Ciotti L., Pellegrini S., Renzini A., D'Ercole A., 1991, *ApJ*, 376, 380

Cole S., Lacey C., 1996, *MNRAS*, 281, 716

Courteau S., Rix H., 1999, *ApJ*, 513, 561

Cunha K., Lambert D. L., 1994, *ApJ*, 426, 170

Dalcanton J. J., Spergel D. N., Summers F. J., 1997, *ApJ*, 482, 659

Dame T. M., 1993, in *AIP Conf. Proc. 278: Back to the Galaxy The Distribution of Neutral Gas in the Milky Way.* pp 267–278

de Grijp R., Kregel M., Wesson K. H., 2001, *MNRAS*, 324, 1074

de Jong R. S., 1996, *A&A*, 313, 377

Dehnen W., Binney J., 1998, *MNRAS*, 294, 429

Dopita M. A., Ryder S. D., 1994, *ApJ*, 430, 163

Dragicevich P. M., Blair D. G., Burman R. R., 1999, *MNRAS*, 302, 693

Efstathiou G., 2000, *MNRAS*, 317, 697

Esteban C., Garcia-Rojas J., Peimbert M., Peimbert A., Ruiz M. T., Rodriguez M., Carigi L., 2004, ArXiv Astrophysics e-prints

Fall S. M., Efstathiou G., 1980, *MNRAS*, 193, 189

Ferguson H. C., Dickinson M., Giavalisco M., Kretchmer C., Ravindranath S., Idzi R., Taylor E., Conselice C. J., Fall S. M., Gardner J. P., Livio M., Madau P., Moustakas L. A., Papovich C. M., Somerville R. S., Spinrad H., Stern D., 2004, *ApJ*, 600, L107

Firmani C., Avila-Reese V., 2000, *MNRAS*, 315, 457

Flores R., Primack J. R., Blumenthal G. R., Faber S. M., 1993, *ApJ*, 412, 443

Flynn C., Fuchs B., 1994, *MNRAS*, 270, 471

Freeman K. C., 1970, *ApJ*, 160, 811

Freudenreich H. T., 1998, *ApJ*, 492, 495

Gilmore G., Wyse R. F. G., Kuijken K., 1989, in *Evolutionary Phenomena in Galaxies Stellar dynamics and Galactic evolution.* pp 172–200

Giovagnoli A., Tosi M., 1995, *MNRAS*, 273, 499

Gould A., Bahcall J. N., Flynn C., 1996, *ApJ*, 465, 759

Guesten R., Mezger P. G., 1982, *Vistas in Astronomy*, 26, 159

Gunn J. E., 1982, in *Astrophysical Cosmology Proceedings The evolution of galaxies.* pp 233–259

Gunn J. E., Gott J. R. I., 1972, *ApJ*, 176, 1

Haywood M., 2001, *MNRAS*, 325, 1365

Haywood M., Robin A. C., Creze M., 1997, *A&A*, 320, 440

Heavens A., Panter B., Jimenez R., Dunlop J., 2004, *Nature*, 428, 625

Helmi A., Navarro J. F., Nordstrom B., Holmberg J., Abadi M. G., Steinmetz M., 2005, ArXiv Astrophysics e-prints

Hernández X., Avila-Reese V., Firmani C., 2001, *MNRAS*, 327, 329

Hernandez X., Valls-Gabaud D., Gilmore G., 2000, *MNRAS*, 316, 605

Hirashita H., Burkert A., Takeuchi T. T., 2001, *ApJ*, 552, 591

Holmberg J., Flynn C., 2004, *MNRAS*, 352, 440

Hou J. L., Prantzos N., Boissier S., 2000, A&A, 362, 921

Hunter D. A., Elmegreen B. G., Baker A. L., 1998, ApJ, 493, 595

Ibata R. A., Wyse R. F. G., Gilmore G., Irwin M. J., Suntzeff N. B., 1997, AJ, 113, 634

Jahreiß H., Wielen R., 1997, in ESA SP-402: Hipparcos - Venice '97 The impact of HIPPARCOS on the Catalogue of Nearby Stars. The stellar luminosity function and local kinematics. pp 675–680

Jimenez R., Padoan P., Matteucci F., Heavens A. F., 1998, MNRAS, 299, 123

Jørgensen B. R., 2000, A&A, 363, 947

Karatas Y., Bilir S., Schuster W. J., 2005, ArXiv Astrophysics e-prints

Kennicutt R. C., 1989, ApJ, 344, 685

Kennicutt R. C., 1998, ApJ, 498, 541

Kent S. M., Dame T. M., Fazio G., 1991, ApJ, 378, 131

Kerr F. J., Lynden-Bell D., 1986, MNRAS, 221, 1023

Kilian J., Montenbruck O., Nissen P. E., 1994, A&A, 284, 437

Kim W., Ostriker E. C., 2001, ApJ, 559, 70

Kim W., Ostriker E. C., Stone J. M., 2003, ApJ, 599, 1157

Korchagin V. I., Girard T. M., Borkova T. V., Dinescu D. I., van Altena W. F., 2003, AJ, 126, 2896

Kuijken K., Gilmore G., 1989, MNRAS, 239, 571

Kuijken K., Gilmore G., 1991, ApJ, 367, L9

López-Corredoira M., Cabrera-Lavers A., Garzón F., Hammersley P. L., 2002, A&A, 394, 883

Lacey C., Cole S., 1994, MNRAS, 271, 676

Lacey C. G., Fall S. M., 1985, ApJ, 290, 154

Larson R. B., 1972, Nature Physical Science, 236, 7

Linsky J. L., 2003, Space Science Reviews, 106, 49

Lubowich D. A., Pasachoff J. M., Balonek T. J., Millar T. J., Tremonti C., Roberts H., Galloway R. P., 2000, Nature, 405, 1025

Lynden-Bell D., 1975, Vistas in Astronomy, 19, 299

Mao S., Mo H. J., White S. D. M., 1998, MNRAS, 297, L71

Martin C. L., Kennicutt R. C., 2001, ApJ, 555, 301

Martin N. F., Ibata R. A., Bellazzini M., Irwin M. J., Lewis G. F., Dehnen W., 2004, MNRAS, 348, 12

Matteucci F., Chiappini C., 2001, New Astronomy Review, 45, 567

Matteucci F., Francois P., 1989, MNRAS, 239, 885

Mera D., Chabrier G., Schaeffer R., 1998, A&A, 330, 937

Mestel L., 1963, MNRAS, 126, 553

Meyer D. M., Jura M., Cardelli J. A., 1998, ApJ, 493, 222

Meza A., Navarro J. F., Abadi M. G., Steinmetz M., 2004, ArXiv Astrophysics e-prints

Molla M., Ferrini F., Diaz A. I., 1997, ApJ, 475, 519

Newberg H. J., Yanny B., Rockosi C., Grebel E. K., Rix H., Brinkmann J., Csabai I., Hennessy G., Hindsley R. B., Ibata R., Ivezić Z., Lamb D., Nash E. T., Odenkirchen M., Rave H. A., Schneider D. P., Smith J. A., Stolte A., York D. G., 2002, ApJ, 569, 245

Nordström B., Mayor M., Andersen J., Holmberg J., Pont F., Jørgensen B. R., Olsen E. H., Udry S., Mowlavi N., 2004, A&A, 418, 989

Olling R. P., Merrifield M. R., 2001, MNRAS, 326, 164

Ostriker J. P., Thuau T. X., 1975, ApJ, 202, 353

Ostriker J. P., Tinsley B. M., 1975, ApJ, 201, L51+

Pagel B. E. J., 1997, Nucleosynthesis and chemical evolution of galaxies. Nucleosynthesis and chemical evolution of galaxies /B. E. J. Pagel. Cambridge : Cambridge University Press, 1997. ISBN 0521550610

Pagel B. E. J., Patchett B. E., 1975, MNRAS, 172, 13

Pagel B. E. J., Tautvaisiene G., 1995, MNRAS, 276, 505

Pardi M. C., Ferrini F., 1994, ApJ, 421, 491

Pierce M. J., Tully R. B., 1992, ApJ, 387, 47

Pohlen M., Dettmar R.-J., Lütticke R., 2000, A&A, 357, L1

Portinari L., Chiosi C., 1999, A&A, 350, 827

Portinari L., Chiosi C., 2000, A&A, 355, 929

Prantzos N., Aubert O., 1995, A&A, 302, 69

Prantzos N., Silk J., 1998, ApJ, 507, 229

Quirk W. J., 1972, ApJ, 176, L9+

Rana N. C., 1991, ARA&A, 29, 129

Ravindranath S., Ferguson H. C., Conselice C., Giavalisco M., Dickinson M., Chatzichristou E., de Mello D., Fall S. M., Gardner J. P., Grogan N. A., Hornschemeier A., Jogee S., Koekemoer A., Kretchmer C., plus three more 2004, ApJ, 604, L9

Reid M. J., 1993, ARA&A, 31, 345

Robertson B., Yoshida N., Springel V., Hernquist L., 2004, ApJ, 606, 32

Robin A. C., Creze M., Mohan V., 1992, ApJ, 400, L25

Robin A. C., Reylé C., Derrière S., Picaud S., 2003, A&A, 409, 523

Rocha-Pinto H. J., Maciel W. J., 1996, MNRAS, 279, 447

Rocha-Pinto H. J., Maciel W. J., Scalo J., Flynn C., 2000, A&A, 358, 850

Rocha-Pinto H. J., Scalo J., Maciel W. J., Flynn C., 2000a, ApJ, 531, L115

Rocha-Pinto H. J., Scalo J., Maciel W. J., Flynn C., 2000b, A&A, 358, 869

Rolleston W. R. J., Smartt S. J., Dufton P. L., Ryans R. S. I., 2000, A&A, 363, 537

Romano D., Matteucci F., Salucci P., Chiappini C., 2000, ApJ, 539, 235

Ruphy S., Robin A. C., Epcstein N., Copet E., Bertin E., Fouque P., Guglielmo F., 1996, A&A, 313, L21

Sackett P. D., 1997, ApJ, 483, 103

Salpeter E. E., 1955, ApJ, 121, 161

Sanders D. B., Solomon P. M., Scoville N. Z., 1984, ApJ, 276, 182

Schaye J., 2004, ApJ, 609, 667

Sembach K. R., Wakker B. P., Tripp T. M., Richter P., Kruk J. W., Blair W. P., Moos H. W., Savage B. D., Shull J. M., York D. G., Sonneborn G., Hébrard G., Ferlet R., Vidal-Madjar A., Friedman S. D., Jenkins E. B., 2004, ApJS, 150, 387

Siebert A., Bienaymé O., Soubiran C., 2003, A&A, 399, 531

Slyz A. D., Devriendt J. E. G., Silk J., Burkert A., 2002, MNRAS, 333, 894

Sofia U. J., Meyer D. M., 2001, ApJ, 554, L221

Sommer-Larsen J., 1991, MNRAS, 249, 368

Tammann G. A., Loeffler W., Schroeder A., 1994, ApJS, 92, 487

Tegmark M., et al. 2004, Phys. Rev. D, 69, 103501

Tinsley B. M., 1980, Fundamentals of Cosmic Physics, 5, 287

Toomre A., 1964, ApJ, 139, 1217

Tosi M., Steigman G., Matteucci F., Chiappini C., 1998, ApJ, 498, 226

Trujillo I., Forster Schreiber N. M., Rudnick G., Barden M., Franx M., Rix H., Caldwell J. A. R., McIntosh D. H., Zirm A., Haussler B., van Dokkum P. G., Labbe I., Moorwood A., four authors more 2005, ArXiv Astrophysics e-prints

van den Bergh S., 1962, AJ, 67, 486

van den Bergh S., McClure R. D., 1994, ApJ, 425, 205

van der Kruit P. C., 1979, A&AS, 38, 15

van der Kruit P. C., 1986, A&A, 157, 230

van der Kruit P. C., 1987, A&A, 173, 59

van der Kruit P. C., Searle L., 1981a, A&A, 95, 116

van der Kruit P. C., Searle L., 1981b, A&A, 95, 105

Wakker B. P., Howk J. C., Savage B. D., van Woerden H., Tufte S. L., Schwarz U. J., Benjamin R., Reynolds R. J., Peletier R. F., Kalberla P. M. W., 1999, Nature, 402, 388

Wakker B. P., Savage B. D., Sembach K. R., Richter P., Meade M., Jenkins E. B., Shull J. M., 2003, ApJS, 146, 1

Wang B., Silk J., 1994, ApJ, 427, 759

Wielen R., 1977, A&A, 60, 263

Wong T., Blitz L., 2002, ApJ, 569, 157

Wyse R. F. G., Gilmore G., 1992, AJ, 104, 144

Wyse R. F. G., Silk J., 1989, ApJ, 339, 700

Young J. S., Scoville N. Z., 1991, ARA&A, 29, 581

Zheng Z., Flynn C., Gould A., Bahcall J. N., Salim S., 2001, ApJ, 555, 393